DOCTORAL THESIS

Modeling of Cold Pilgering of Stainless Steel Tubes

Yağız Azizoğlu

Solid Mechanics

LULEÅ UNIVERSITY OF TECHNOLOGY

Modeling of Cold Pilgering of Stainless Steel Tubes

Yağız Azizoğlu

Division of Mechanics of Solid Materials
Department of Engineering Science and Mathematics
Luleå University of Technology
SE-97 187 Luleå, Sweden

Doctoral Thesis in Solid Mechanics

ISBN:
ISBN: (print)
ISBN: (pdf)

Published:
Printed by Universitetstryckeriet
Luleå University of Technology

www.ltu.se

Acknowledgments

First of all, I would like to thank my supervisor, Professor Lars-Erik Lindgren for his excellent guidance and support. I am also grateful to Mattias Gärdsback, Mathias Hareland and Tomas Jansson for their valuable suggestions in the modeling part. I would like to thank Zhili Song for sharing his PhD experience and encouragement. I am thankful to Bengt Sjöberg for his generous support and supervision in the experimental part. I also wish to extend my thanks to Stefan Björk, Per Dürebrandt and Peter Nordin for their support in the experimental part.

Furthermore, I would like to express my gratitude to friends and colleagues at Alleima (previously Sandvik Materials Technology), Dalarna University and Luleå University of Technology for creating friendly environment.

Finally, I would like to thank my family and my friends for their support.

This work was performed within the Swedish Steel Industry Graduate School with financial support from Alleima, Högskolan Dalarna, Region Dalarna, Region Gävleborg, Länsstyrelsen Gävleborg, Jernkontoret and Sandviken kommun.

Abstract

Cold pilgering is a complex forming process used to produce seamless tubes in terms of modeling due to the complexity in kinematic of tools, friction condition and material behavior. The process development has mostly been based on simple formulas and costly full-scale tryouts. The aim in this study is to develop validated Finite element models of cold pilgering to support design of a robust process.

A three-dimensional thermo-mechanical Finite element models of cold pilgering has been developed in the course of the work leading to this thesis. The commercial code MSC.Marc was used in the simulations. General 3D models are needed to be able to capture asymmetric deformation in cold pilgering. Elastic deflections of tools and roll stand were included in the model via linear and nonlinear springs that were calibrated versus experiments. A temperature dependent Chaboche type plasticity model was employed in this simulation to mimic strain hardening and softening behavior under multidirectional loading. The model parameters were optimized using multi-directional compression and uni-directional tensile tests. Heat exchange between tools and lubricant was included in the simulation via heat convection films on the surfaces. The film parameters were calibrated using experimental data. Simulation predictions for hardening, rolling force, process temperature and geometry were compared with experiments for validation purposes. The predictions showed overall good agreement with validation experiments enabling the use of this model for understanding and improving the process.

Keywords: Cold pilgering, finite element method, tube forming, tool elasticity, Chaboche plasticity

Thesis

This is a compilation thesis consisting of a synopsis and the following scientific articles:

Paper I
Finite Element Modelling of Cold Pilgering of Tubes
Y. Azizoğlu ; M. Gärdsback ; B. Sjöberg ; L-E. Lindgren
COMPLAS, International Conference on Computational Plasticity, 2015, pp.716-726

Paper II
Finite element modeling of tube deformation during cold pilgering
Y. Azizoğlu ; M. Gärdsback ; B. Sjöberg ; L-E. Lindgren
MATEC, Vol. 80, 2016, article id 15004

Paper III
Finite Element Analysis of cold pilgering using elastic roll dies
Y. Azizoğlu ; M. Gärdsback ; B. Sjöberg ; L-E. Lindgren
Procedia Engineering, Volume 207, 2017, Pages 2370-2375

Paper IV
Work hardening during alternating load direction of 316L SS
Y. Azizoğlu ; M. Gärdsback ; A. Yamanaka; T. Kuwabara; L-E. Lindgren
Procedia Manufacturing, Volume 15, 2018, Pages 1777-1784

Paper V
Temperature and plastic strain dependent Chaboche model for 316L used in simulation of Cold Pilgering.
Y. Azizoğlu and L-E. Lindgren
Submitted for journal publication

Paper VI
Modeling of cold pilgering of stainless-steel tubes
Y. Azizoğlu ; B. Sjöberg ; L-E. Lindgren
Submitted for journal publication

Author's contribution
The present author was responsible for conducting all the experimental and modelling work, and for writing the presented articles.

Contents

1 Introduction

1.1 Outline

The objective of the work presented in this thesis is to evaluate and develop a validated model for the cold pilgering process that can be used to predict rolling force, process temperature and work hardening with sufficient accuracy to support design decisions. In the introduction chapter, the motivation and aim of this study are presented. The second chapter introduces important aspects and parameters in the cold pilgering process. A review of used modeling approaches is given in chapter three. The fourth chapter gives a summary of developments in the course of this work. Chapter five includes conclusions together with suggestions for future work.

1.2 Background

Cold pilgering is a cold forming method that is employed to produce high precision seamless tubes that have tight geometric tolerances and high surface quality. In this forming process, the tube preform is repeatedly compressed between a stationary mandrel on the inside and two rolls on the outside. After each stroke, tube preform is fed forward a small distance and rotated around its axis. These small forming steps enable to progressively reduce the diameter and wall thickness according to the profiles of the mandrel and the roll dies. For some materials total area reduction of 90% can be reached [1]. The large area reduction and the friction between the metal surfaces generate a significant amount of heat. The tube surface is continuously lubricated by oil jets that dissipate this heat and decrease friction. The latter does also reduce generated heat as well as improves surface quality.

The main strategy in most metal forming processes is to produce maximum amount of the product in a unit time by minimum tool usage. Process optimization is a very important part of metal forming process to reach this goal and a thorough understanding of influence of process parameters is then needed. Some important variables in metal forming are strain history, flow stress and temperature in the work piece, as well as contact pressure and friction in the interface between the work piece and the tool. Those parameters help predicting maximum load in the tool, mechanical properties of the final product and process temperature.

During the last decades, computational methods have become more common used when evaluating metal forming processes [2]. The reason is that forming machines and processes are commonly too complex and too expensive in order to perform measurements or tryouts. The finite element method (FEM) has become the most common numerical method in this respect. It gives a possibility to evaluate the effect of various process parameters on the properties of the formed tube and thus increases the understanding of the process. However, it is still a complex and computationally challenging task.

1.3 Aim of research

The aim of the research is to develop validated finite element (FE) models of the cold pilgering process of stainless-steel tubes in order to support design of a robust process. Important parameters in design process are mainly rolling force, process temperature, geometric evolution and mechanical properties of the final tube. Experiments will be performed both to validate FE models and calibrate various parts of the model. The overall encompassing research question can be phrased as,

"How should a sufficient accurate finite model of the cold pilgering process of tubes be formulated in order to be useful for design of the process?".

1.4 Research questions and limitations

The literature review and experience at Alleima Ltd (Previously Sandvik Material Technology) have led to the following specific questions to answer in order to fulfill the general aim in the previous section.

Research questions:

R1. What improvements of existing models are needed to better predict rolling force, process temperature, geometric evolution of workpiece and mechanical properties of the final tube?
R2. What macro-scale material model can mimic work hardening in the cold pilgering process?
R3. What mechanical testing and material parameter optimization methods are needed to the model in R2?
R4. What experiments are needed to calibrate and validate the developed models?

The developed model is limited to the Vertical Mass Ring Die (VMR) type of cold pilgering process for stainless-steel tubes. This process is explained in the next chapter. The material model is optimized for 316L type of steel. However, it could be optimized and used for other

steel grades. The used macro-scale modeling approach cannot account for texture evolution. This limits what mechanical properties of the tube can be predicted.

2 The cold pilgering process

Development of rolling mill technology during the first half of 19th century facilitated the industrial manufacturing of tubes and pipes. They were first manufactured by forming rolled strips of sheets into circular cross sections and then welded along the edges. Methods to manufacture seamless tubes and pipes were later developed. They almost completely dominated the market until effective welding methods were developed. Presently, around one third of the manufactured steel tubes and pipes are seamless. They are preferred for tubes with wall thickness between 1.6 – 14.2 mm and outer diameters of 10.2 – 660 mm [3].

Cold pilgering is one of two major method used in seamless tube production. The initial concept of pilgering was developed by Mannesmann brothers in 1880 [4]. This concept was used for hot tube manufacturing process. Since then, many individuals and companies from all over the world contributed to the development of the cold pilgering process. In 1931, a company, Meer of Germany, was granted the patent right of cold pilgering. The other major method is cold drawing but cold pilgering has several advantages that are [4-6]

- high production rate (up to 6 m/min for stainless steels),
- decrease in eccentricity (30-50 % improvement),
- large area reduction (up to 70-90 % for different metals),
- narrow dimensional tolerance (variations of less than 10 μm can be achieved),
- high surface quality (R_a values $\leq$0.4 μm can be achieved) and
- improving the grain structure of the material.

This method is suitable for the most metals however different metals exhibit different maximum area reductions. This type of high precision tubes are demanded in a wide range of industries e.g., oil and gas, nuclear, medical, aerospace etc. [4].

There are two common techniques of cold pilgering which are HPTR (High Precision Tube Roller) and VMR. The main difference between these methods is that HPTR has constant cross-sections of groove and mandrel, whereas VMR has much more complicated groove and

mandrel design where the cross-sections vary along the rolling direction. This complex design enables higher output rates and makes VMR the most common technique. However, HPTR is preferred for some specific applications such as for tubes with extreme diameter-to-wall-thickness (D/t) ratios, larger than 100/1, for nuclear fuel cladding [7].

A typical cold pilgering production line consists of five main sections (see Figure 1).

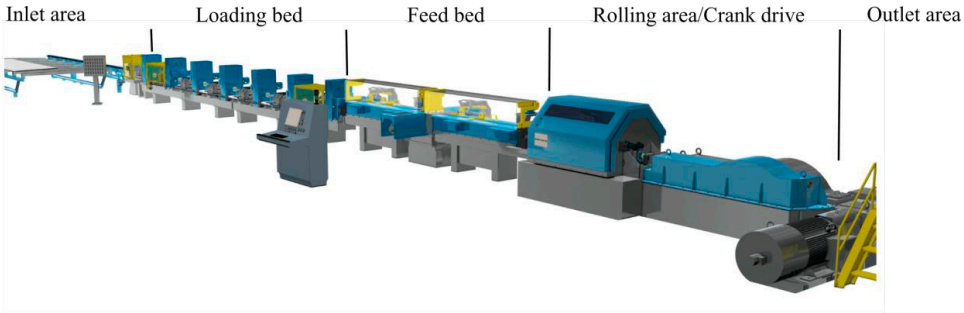

Figure 1: Cold pilgering mill sections [5].

The first section is the inlet area where preforms are installed to the mill. The second section is the loading bed used for loading preforms to the feed bed. The hydraulic clamp of the mandrel rod (mandrel chuck) is located in this area. The third section is the feed bed in which the hydraulic clamp of the preform (feed chuck) is located. The next section is the rolling area (forming section) where cold forming is performed. In this section, the crank drive is also located which gives the oscillating motion to the roll stand. The last section is the outlet area where the finished tubes leave the mill.

The basic idea of this method is to reduce both the diameter and the wall thickness of the tube preform and improving the grain structure of the material. The tube wall thickness is reduced and simultaneously it becomes elongated. The elongation contributes to the productivity of the method and is directly related to the amount of area reduction applied. This depends on the mandrel and roll die design and motions.

The preform, obtained from a previous extrusion process [8], is subjected to repeated compression sequences between a stationary conical mandrel and two vertical roll dies. They are moving back and forth, called a stroke as indicated in Figure 2. The tube is fed a small amount, commonly 1-10 mm, forward and rotated a certain degree when the rolls are at the inlet and/or outlet positions. They are not in contact with the groove at these locations by means of special design of dies. The use of many, small feeding steps ensures a large area reduction without initiating cracks. The preform has a certain amount of eccentricity, which is not desired in high precision tubes. Furthermore, the tube is ovalised during the

compressions in the cold pilgering process due to the side relief of grooves. The rotation steps are therefore applied so that the eccentricity and ovality are reduced until a virtually homogeneous wall thickness is obtained.

The mandrel is connected to a mandrel rod, see Figure 2, which is supported by a mandrel chuck (hydraulic clamp). This chuck is used to prevent the axial movement of the rod and also rotate it after strokes. The preform is supported by a feed chuck. Similarly, this chuck is used to prevent the axial movement and also feed/rotate the preform after strokes. Roll dies are housed within a roll stand (also called a saddle), which moves back and forth. This motion is controlled by a crank drive system. The finished tube is supported by an outlet chuck to prevent vibrations and bending due to the gravity. Moreover, the tube surface is continuously lubricated by oil jets to decrease the temperature due to heat generated.

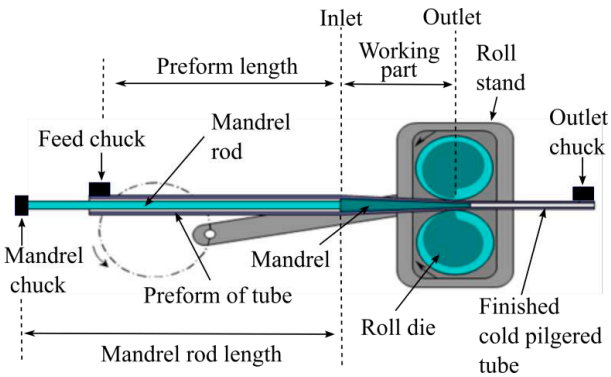

Figure 2: Illustration of the pilger mill.

The process parameters feed and stroke rates plus rotation steps, together with the lubrication state and tool parameters the evolution of plastic strains in the tube. This plastic strain history determines the obtained tube geometry and loading and lubrication conditions determine surface quality. Typical tolerances on the outside diameter and wall thickness of the tube are 0.75% and 10% [9]. Thus, the model needs to be able to predict influence of process parameters on these variables with a high precision.

The following subchapters contain descriptions of more details of various parts of the pilger mill together with existing and design concepts.

2.1 Mandrel and roll dies

Since the pilgering tools determine the shape of the pilgering cone and the final tube, they are the most important and complex elements of the cold pilgering operation. The tools consistent of a mandrel and two roll dies. They determine the inner diameter (ID) and outer

diameter (OD) reductions of the preform, respectively. The forming operation is performed within two sections; the working section, where the OD/ID of the preform is progressively reduced, and the sizing section where the ovality of the tube is decreased without area reduction, see Figure 3.

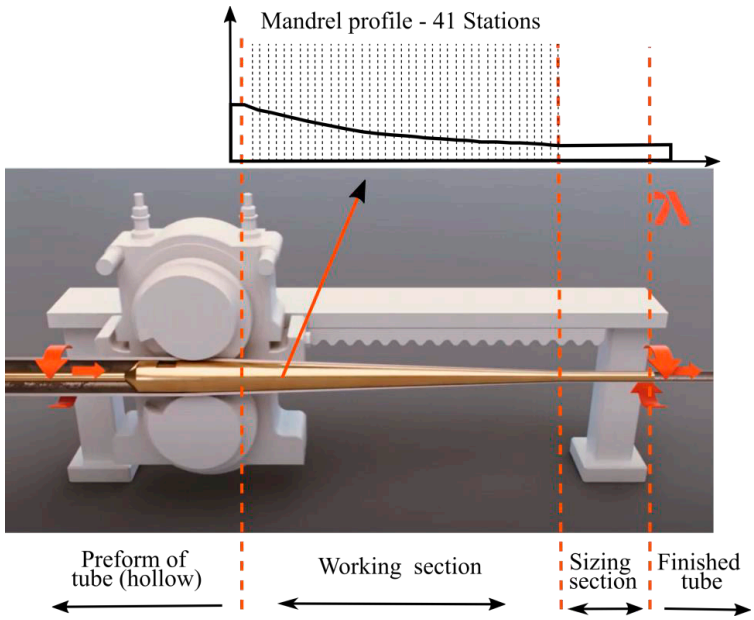

Figure 3: Forming section and mandrel stations.

There are two common designs for the mandrel and roll dies: straight or curved taper [4]. In this study, the curved design is studied as it enables higher reduction rates. The mandrel has a conical shape with decreasing diameter in the working section and a constant diameter in the sizing section, see Figure 3. The working section consists of 41 stations where tool making technology is the limiting factor to machine the curved tool design. The mandrel diameters at these stations are calculated using power-law functions, e.g. Eq.1 [10].

$$OD_{mandrel}(X)=ID_{finish\ tube}+(ID_{preform}-ID_{finish\ tube})(1-X/L)^{M_1} \quad (1)$$

In this equation M_1 is a design parameter of the mandrel, L is the length of the mandrel and X is the mandrel position.

Roll dies have grooved surfaces, see Figure 4, which force the preform against the mandrel to determine OD. The groove consists of approximate half-circle cross sections around the roll die. Similar to mandrel, there are 41 stations in the working section, where the groove radius

decreases from the first station to the last station. In the sizing section, on the other hand, the groove radius is constant. The groove stations coincide with the mandrel stations where the gap between the reciprocal stations determines the amount of area reduction in each station. These incremental area reductions over the sections enable a progressive area reductions leading to a large total reduction.

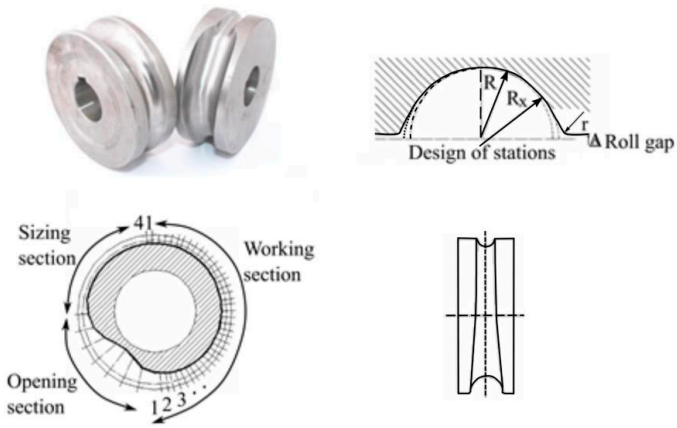

Figure 4: Roll dies.

The cross sections of the groove are not fully circular but slightly oval. In addition to a base groove profile, *R* in Figure 4, there are side relief clearances in the flange parts. Side relief is desired to circulate the lubricant and accommodate elongation due to area reduction in the groove part. Without this clearance, hydrostatic stress states can be generated all around the cross section and the tube can get stuck onto the mandrel. However, it also causes ovalisation of tube, which must be corrected in the working and sizing sections.

The cross sections are constructed using three arcs. The first arc, *R* in Figure 4, determines the base groove, which is calculated using Eq. 2 [10]. The other two arcs, R_x in Figure 4, evaluate the side relief clearances.

$$2R_{groove}(X)=OD_{finish\ tube}+(OD_{preform}-OD_{finish\ tube})(1-X/L)^{M_2} \quad (2)$$

In addition to working and sizing sections, there is an opening part in the groove, in which the groove and the tube has no contact (see Figure 4). This part is used to enable feeding and rotating the preform when the rolls are at the inlet and outlet positions.

There are various considerations when the design parameters are evaluated. The M_1 and M_2 values give the mandrel and roll die curves. They determine the area reduction and elongation

rates. Stress and strain histories, hardening rate, yield and tensile strength and crystallographic texture of the tube are strongly depended on the tool design. Moreover, forces on the tool and hence surface quality and tool life are also strongly dependent on the tool design [4]. The dimensional accuracy, eccentricity and ovality, can be improved by appropriate tool design. It is necessary to optimize the design parameters considering the desired microstructure, mechanical and surface properties and also with a reduced tool wear.

Elongation is a common measure of productivity in cold pilgering and is a consequence of the area reduction. Workability of the material is a limiting factor for maximum area reduction. Abe *et al.* [11] developed a method to evaluate the workability of the Zr alloy tubes. In this method, specimens are taken from three directions in the tube preform. Later, compression tests are performed on this specimen to determine the maximum reductions in height before crack is initiated. They showed that the circumferential ultimate reduction in height is related to formation of fissures.

In addition to area reduction, reduction mode and Q-factor have also a great influence on fissure/crack formation, reported in several studies. The Q-factor is the ratio between the reduction of the wall thickness and the diameter reduction. Abe *et al.* [12] in 2012 made series of cold pilgering trials for three different preform materials, austenitic stainless steel, duplex steel and Ti alloy. For these trials they used various Q-factors in different passes, P1-P5, which are 0.7, 1.1, 1.5, 2.4, 4.2, respectively. The percentage of area reduction is the same for all passes. The result showed that increasing the Q-factor decreases the formation of fissures.

Abe *et al.* [10] in 1994 performed cold pilgering trials for zircaloy-2 tubes with various Q-factors to examine crack formation on the tube surface in addition to numerical calculations using the model in [13]. They observed cracks on the tube surfaces that have a larger quotient between the circumferential compressive and radial tensile strains, i.e. larger $-\varepsilon_r/\varepsilon_\varphi$. This was extra clear in the flange part, see Figure 5. They concluded that for less workable material a higher Q-factor should be used.

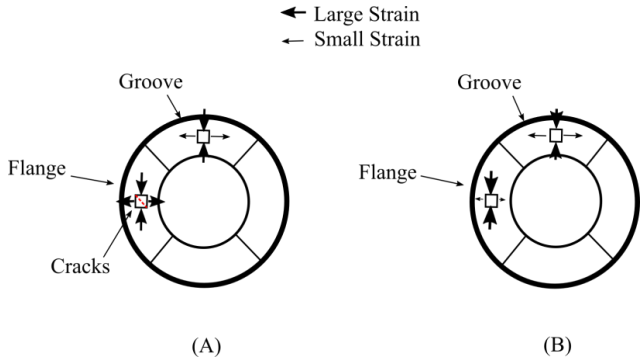

Figure 5: Schematic diagram of crack mechanism: a) bad pilgering, b) good pilgering, modified from [10].

Abe *et al.* [12] claimed that a low strain ratio, $-\varepsilon_r/\varepsilon_\varphi$, in the flange part is an indicator of good cold pilgering conditions. They experimentally observed that larger strain ratios cause deeper fissures. Harada *et al.* [14] and Girard *et al.* [15] evaluated the influence of tool design on the damage evaluation using numerical simulations. Furugen *et al.* [13] used 2D/3D models to optimize tool shape by considering minimum energy consumption criteria. Montmitonnet *et al.* [16] found from their experiments that the tool design influences the internal surface topology of the tube.

Abe *et al*. in 2000 [17] conducted both numerical and experimental investigations to examine the influence of the tool design parameter, M_2 in Eq. (2), on the tube quality and tool loads. A numerical model was used [13] to calculate the stress and strain of the preform in both the groove and flange parts of the cross sections. They also computed the loads on the tool for different M_2 values. The results showed that increasing M_2 increases the peak values of strains and shifts the peak forward in the axial direction.

In the experimental part, they used two different roll die designs, denoted A and B, with different groove curves. They calculated axial strains for these grooves and observed abrupt changes in design B. They obtained a defect free surface with roll die design A but circumferential cracks were observed using roll die design B. They concluded that abrupt changes in the axial strain caused the cracks. Therefore, it is desired to have smooth changes of the working sections to prevent surface defects. This can be ensured by lowering M_2. However, this decreases tool life on the other hand.

Furthermore, texture development is influenced by the design parameters [18]. There are two common methods to characterize the texture. First is using inverse pole figures by x-ray diffraction [19]. Another method is measuring anisotropy in plastic deformation because of crystallographic texture [20]. In this method, Contractile Strain Ratio (CSR) test is used to

investigate the degree of developed texture. CSR value is measured by the ratio of true circumferential strain, ε_c, at the mid-wall location and true radial strain, ε_r. The correlation between the Q-factor and these values was reported in early studies [12,20]. Therefore this parameter, hence the texture in the tube, is influenced by changing the Q-factor.

Additionally, the tool design influences the oil film thicknesses between the tools and tube, hence the friction changes [21]. Abe *et al.* [21] in 2014, calculated oil film thickness for different design parameters, M_1 and M_2, using Reynolds equation [22]. They calculated oil film thicknesses over the working section for different design parameters at the outer and inner side of the tube. They concluded that the tool design parameters have large influence on the oil film thickness. In addition, they pointed the important of side relief design on the lubrication state, particularly for large feed steps.

The estimation of the side relief clearance is very important in the tool design process. It affects the plastic deformation state and the dimensional accuracy of the final tube very much. Too large clearance can cause wear on the tube and tool.

2.2 Kinematics of tools

Selection of process parameters are, in addition shape of tools, important in order to ensure the desired microstructure, mechanical and surface properties while preserving the tool life. They are related to the kinematic of the tools, feed and stroke rates as well as rotating increments.

Roll dies are housed inside a saddle, Figure 6, where they are connected to pinion gears.

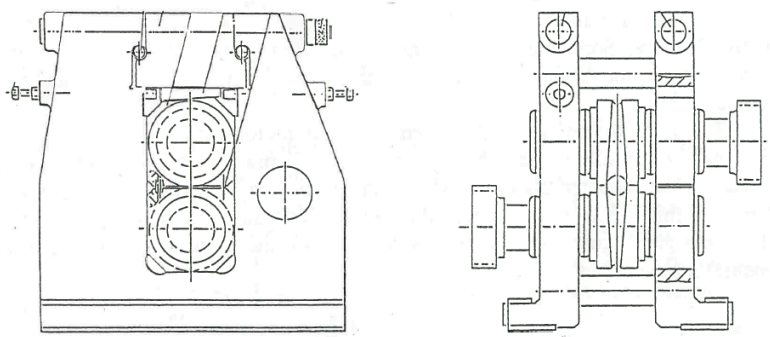

Figure 6: Saddle view [4].

These gears are interlocked with gear rocks which are fixed on the machine frame so that the Rack and Pinion system, see Figure 7, ensures rolling without sliding movement of the rolls.

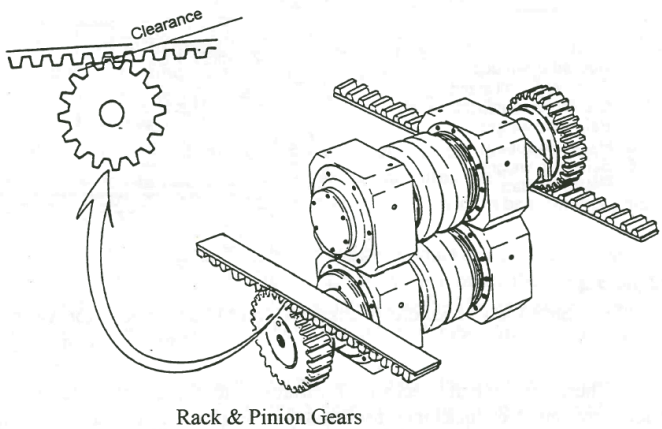

Figure 7: Rack and pinion gears [4].

The saddle is moved back and forth to provide pilgering strokes. This movement is given by a crank drive system, see Figure 8, via a connecting rod to the rolling stand (saddle). There are two major moving balance weights that are positioned either vertically or horizontally. In this study, vertical movement is subjected.

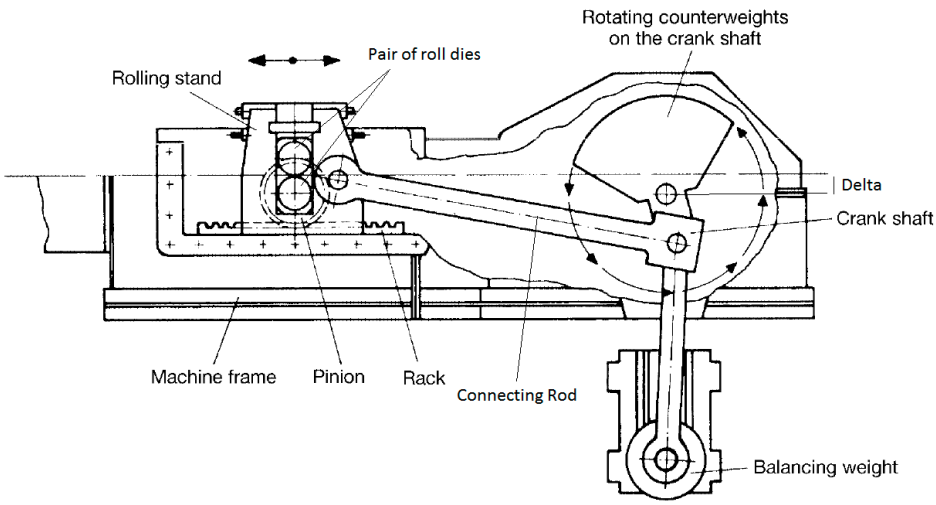

Figure 8: Roll stand and crank mill [3].

The stroke length, l, is calculated by Eq. 3 where L is the length of the connecting rod, r is the radius of the crank circle and delta, δ, is the offset of the crank drive. Normally the stroke length is smaller than the circumference of pinion pitch. The leads to that the pinion gear never comes in contact with the gear rock for some turning angles.

$$l = \sqrt{(L+r)^2-\delta^2} - \sqrt{(L-r)^2-\delta^2} \tag{3}$$

In the opening part, when the rolls are at the inlet or outlet position, the preform is fed forward towards the working section using the feed chuck, see Figure 2, a small amount (commonly 1-10 mm). Small feed steps, hence the deformation steps, are desired to reach high area reduction without initiating cracks. The feeding amount per stroke is called "feed rate" which is the first process parameter. In addition to the feeding, the preform is also rotated around the axial direction using the same chuck a certain degree after strokes. These turning steps are desired to enhance ovalisation to reach virtually circular cross-sections. The turning amount per stroke is the second process parameter called "turning step".

The number of strokes in a unit time, on the other hand, is the last process parameter called "stroke rate". The stroke rate is evaluated by the axial position, $z(t)$, and velocity, $v(t)$, of the rolling stand which are calculated using Eq.s 4 and 5 [21]. In these equations, $\theta(t)$ is the crank angle at the time t and ω is the angular velocity of the crank.

$$z(t) = \sqrt{(L+r)^2-\delta^2} - \left\{ r.\cos\theta(t) + L - \frac{L}{2}\left(\frac{r.\sin\theta(t)+\delta}{L}\right)^2 \right\} \tag{4}$$

$$v(t) = r.\omega.\left\{ \sin\theta(t) + \frac{r.\sin\theta(t).\cos\theta(t)+\delta.\cos\theta(t)}{L} \right\} \tag{5}$$

The velocities of pinion gears are determined by the saddle velocity and pinion pitch diameter. Even though pinion gears and roll dies have the same angular velocity, tangential velocity of the pinion and the groove differ due to deviation of the roll die radius from the pinion pitch diameter. Figure 9 illustrates this deviation where the red line represents the pinion pitch diameter.

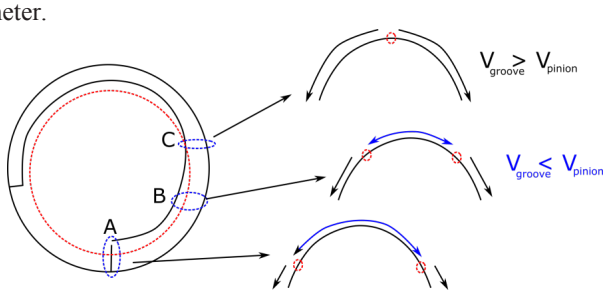

Figure 9: Illustration of the tube and groove velocity.

Cross-sections A-C show intersection points where the groove points, shown by small red circles, are located at a distance from the axis equal to the pinion pitch diameter. The groove points have greater diameters from the intersection points towards the flange part. They have therefore greater tangential velocities than the pinion gear. Contrary, the points between the intersections, shown by blue arrow, have smaller diameters and corresponding lower tangential velocities. After the cross-section C, which is commonly placed near middle of the working section, groove points have always greater diameters than the pinion gear. Yoshida *et al.* [23] expressed the variation of the tangential velocities regarding the shift from the pinion pitch circle using an analytical expression given in Eq. 6. In this equation, υ_R is the longitudinal velocity of a roll at each point, R_p and R_0 are the distance from the roll center to the pinion pitch and the groove shoulder respectively and r_2 is the radius of the base groove.

$$\upsilon_R=(1-\frac{R_0-r_2\cdot\sin\theta}{R_p})\cdot\upsilon_0 \tag{6}$$

The elongation velocity of the material flow is determined by the area reduction rate along the working section. Typically, 75% of the total area reduction occurs within the first 1/3 of the working section [4]. Therefore, is the elongation velocity in this section much higher than in the remainder working sections. Furthermore, material elongation is greater in the flange part of the groove than at the bottom due to restraint from boundaries, described in Sec. 2.3. Yoshida *et al.* [23] assumed that the velocity of material, υ_M in Eq. 7, increases linearly from zero to υ_1, the displacement velocity of reduced tube, along the contact arc, l_d, which varies around the hoop direction.

$$\upsilon_M=\frac{\upsilon_1}{l_d}\cdot x\,,\quad 0\le x\le l_d \tag{7}$$

Rolling without sliding movement of the roll dies occur only when the groove points and material flow have the same tangential velocity. There is a sliding between the surface everywhere else. The associated friction causes shear stresses between the groove and tube. Yoshida *et al.* [23] determined the directions of the relative sliding by υ_R and υ_M in the hoop direction to estimate the friction in the contact area. Integrating the friction stresses over the contact area gives the total friction force. The total friction force in the axial direction creates the so called “push-pull effect”. The roll dies tend to push the tube in the early stages of a stroke, commonly 1/3, and afterwards they pull the tube forward. The axial position, where no push or pull effects occur, is called the “neutral point”. The magnitude of the push-pull effect and location of the neutral point are important. Its location is affected by the groove design and pinion diameter. It should be located to avoid extensive forces on the rolls, mandrel and the feeding tools as well as unintentional self-feeding.

It is preferred to select as high stroke and feed rates as possible within the possible range of process parameters to improve productivity. However, this also increases the deformation

rate, giving larger forces and stresses in the tools. The allowable stress in the tools and risk for cracks thus limits stroke and feed rates. Moreover, larger feed steps gives more deformation during each stroke and generates more heat and a higher stroke rate reduces the available time for cooling between strokes and thereby the temperature increases. A too high temperature can burn the lubricant and then damage the surface. It also lowers the temperature dependent yield strength of the tools. Plastic deformation of the tools shortens their life. Furthermore, the combination of feed rate and rotation increments influence the strain history and thereby texture and mechanical properties of the tube [6].

Additionally, a greater feed rate increases the contact length and width between the tools and tube. A greater length gives a more homogeneous deformation whereas a greater contact width may cause surface defects. This can be the case if it fills the grooves so the relief clearance disappears. Moreover, a greater feed rate causes more ovalisation and the preform is subjected to fewer strokes through the sizing section to improve the circularity of the tube.

There are a few studies in the open literature where the influences of the process parameters are investigated. Girard *et al.* [15] made experimental and numerical investigations examining the influence of feed and stroke rates on the shear strain which is an indicator of damage. They concluded that, without giving the absolute values, 18% increase in the stroke rate decreases the shear strain, ε_{zr}, from 0.43 to 0.38 and increase in the feed rate decreases this strain from 0.43 to 0.39. Abe *et al.* [21] in 2014 investigated the lubrication state by hydrodynamic calculation of the oil film thickness. The calculation was made for three different stroke rates, 140, 180, and 220 strokes/min together with three feed rates, 0.5, 1, and 2 mm/strokes. The oil film thickness increases with increasing stroke rate. This was attributed to the increase of the tube compression velocity which pushes oil towards the contact region, in the oil bite with increasing roll velocity.

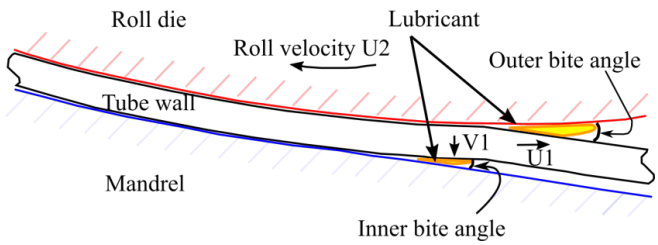

Figure 10: Lubrication state modified from [21].

The oil film thickness on the inner, but not outer, side of the tube was influenced by the feed rate. The reason of was due to that the elongation velocity, U_1 in Figure 10, is much lower than the roll-die velocity, U_2. However, the mandrel is stationary on the inner surface and the tube compression velocity, V_1, is significant. This is an important result as the oil film

thickness significantly influences the friction force and surface quality as explained in Sec 2.5.

Abe *et al.* [24] in 2016 experimentally investigated the influence of process parameters on the residual stress of the tube, roll die gap, ovality and eccentricity. The tested parameters were feed rates of 1.0, 1.5, 2.0, 2.5 mm and stroke rates of 140, 180, 200 strokes/min and turning steps of 40, 60 and 80°. They measured the residual stresses of the finished tubes by using the Crampton method [25]. Results showed that the process parameters affect the residual stress, see Table 1.

Table 1: Residual stress for different process parameters, taken from [24].

No.	Process condition		Residual stress (MPa)	
	Feed rate (mm)	Turn angle ()	316L	Zry4
1	1.0	80	-30.7, -27.8	-15.9, -13.2
2	1.5	80	-9.2, -8.4	+2.7, +1.2
3	2.0	80	-9.2, -9.9	+2.7, +5.0
4	2.5	80	-9.9, -9.2	+5.4, +3.5
5	1.5	60	-26.9, -30.7	-2.3, -1.5
6	1.5	40	-18.4, -15.4	+18.1, +18.1

They also measured the gap between the roll dies during the strokes. They observed that for each increase in the tested feed rate, the gap increases around 0.02 mm. The initial gap between the roll dies because the increasing rolling force during a stroke elastically deforms the roll stand. It is important to take this deflection into account to reach desired OD and wall thickness (WT). Abe *et al.* [24] also showed that the ovality of OD and ID increase with the feed rate. Moreover, ID showed a greater ovality than that of OD due to the differences in their contact areas. However, the stroke rate did not influence the ovality in their experiments. This may be due to insufficient wide maximum strain rates to affect the plastic deformation state. Use of larger turn angles gives a lower ovality. Finally, they claimed that the studied process parameters had no effect on the eccentricity.

2.3 Deformation of tube

The material response to the complex loading naturally gives also a complex plastic flow in the tube together with texture evolution. It is a challenge to understand and evaluate the deformation history even when using numerical tools. However, it is important in order to be able to produce defect free tubes with desired mechanical properties and geometry. It has been reported in the literature that the plastic deformation route affects the formation of fissures [12] and work hardening [26-28]. It is possible to reach the same final state with different routes where some may be better than the others.

The tube cross section is divided into two main deformation regions; the groove and flange parts as illustrated in Figure 11. In the groove part, the work piece is in contact with both the mandrel and the groove. All principal stresses are compressive in this region. The work piece is subject to a large compressive strain in the radial direction and a small tensile strain in the tangential direction. In the flange part, the work piece is in contact only with the groove. The radial stress is compressive (rather small) and the axial stress is tensile. There is a large compressive strain acting in the tangential direction, and a rather small tensile strain in the radial direction. This part is more prone to form fissures [12].

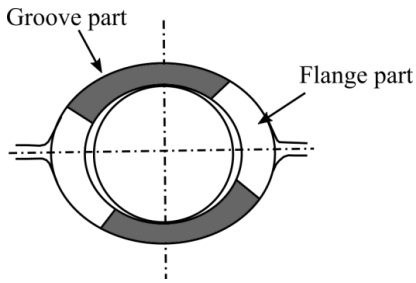

Figure 11: Partition of a tube-section modified from [17].

Several experimental and numerical studies in the literature investigate the stress and strain states. Yoshida *et al.* [23] measured the circumferential distribution of the contact length, rolling pressure, normal strain. They showed that contact lengths, rolling pressures and deformation states vary significantly in the hoop direction which makes the deformation highly complicated and asymmetric. Montmitonnet *et al.* [29] calculated the tangential distribution of principle stresses using 3D FEM of cold pilgering for three strokes and showed the asymmetric stress states in the hoop direction.

In addition to dividing the cross section into the groove and flange part, the deformation region in the longitudinal direction is divided into three main regions. They are called “Squeeze zone”, “Forging zone” and “Bending zone” shown in Figure 12.

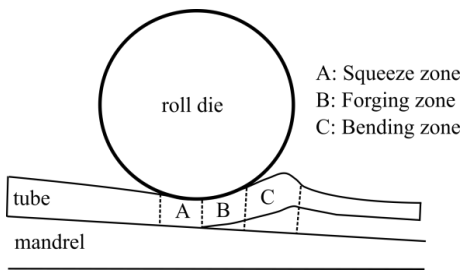

Figure 12: Contact zone.

The material is already rolled down to the mandrel in the squeeze zone. In the forging zone, the material is in contact with both the mandrel and die. The tube surface bends in the Bending zone so it looks like a wave ahead of the roll [14,30,31].

Since the preform is fed forward with small steps and rotated after each stroke, a unit volume of the metal piece undergoes complex, non-proportional multi-axial stress/strain history during the process. Vanegas-Márquezes *et al.* [32] calculated the accumulated strain components after each stroke, see Figure 13. They pointed that even though compression dominates the history the few isolated tensile condition could cause damage and crack.

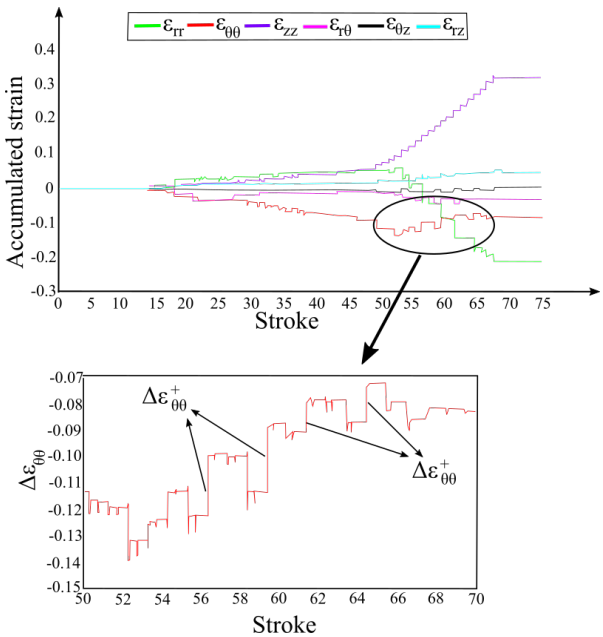

Figure 13: Strain path undergone by of a volume element during HPTR cold pilgering of a cladding tube, adapted from [32].

There are several factors which can influence the material flow, hence the strain history, besides the tool design and process parameters. One of them is that the shear strain near the surface of the tube strongly depends on the friction between the tool [15,31,33]. This is an important factor causing inhomogeneous deformation [34] and surface damage [15,30]. Another factor is the deformation and displacement of the tool that affect the forming process [13,14,24,30,35].

2.4 Lubrication

Lubrication is a key factor in the cold pilgering operation in terms of productivity, as in most metal forming operations. This is due to several reasons. First of all, it preserves the surfaces quality of the tool and tube which is a highly important criterion for cold finishing processes. A bad lubricant increases the friction and accelerates material transfer from the tube surface to the tool surface. Built up material on the tool surface causes scratches on the tube, making it necessary to grind the surface of the tool more often, and reduces tool life [15,16,36]. Secondly, it functions as a coolant to reduce the heat generated by friction between the work piece and the tool [37]. Temperature control is important as a too high temperature may burn the lubricant. Thirdly, it prevents the preform from getting stuck on the mandrel.

The lubrication is supplied in two stages. The inner surface of the preform is lubricated between feeding steps by nozzles installed in a connecting part between the mandrel and mandrel rod. The outer surface is lubricated during the process by oil jets, see Figure 14.

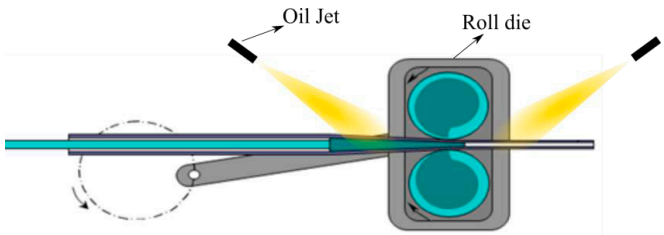

Figure 14: Schematic view of cold pilgering showing jets of lubricant entering the deformation region.

The following criteria are considered when selecting lubricant: lubricity performance, the environmental issues and the corrosion protection [4]. The influence of lubricant and flow on friction and surface topology has been extensively studied in [16,36,38-40].

2.5 Friction

In general, the friction in metal forming operations is an important factor. It dissipates energy, thus increase the needed force for desired deformation. A large fraction of the dissipated energy increases the temperature. Furthermore, it causes wear of the contacting surfaces. Moreover, the material flow and homogeneity of the deformation is affected [15,31,33].

Friction is a complicated phenomenon due to complex micro-scale formations on the interfaces, especially when the lubrication is involved [2,41,42]. There are several factors

influencing the friction such as the contact topology, material properties, relative sliding velocity and the presence of lubrication. The Stribeck curve [43] divided the contact conditions in four regions [42,44]. They are dry, boundary, mixed and hydrodynamic conditions and based on the asperity height and oil film thickness. In this curve, the coefficient of friction and oil film thickness are given as a function of lubricant viscosity, sliding velocity and normal pressure shown in Figure 15.

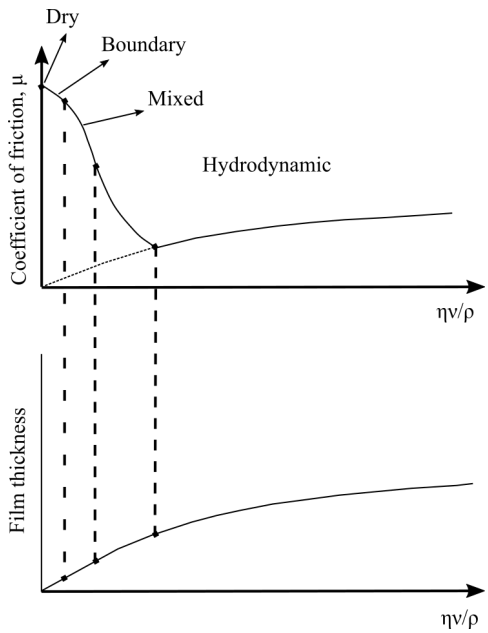

Figure 15: Siebel curve, showing onset of various lubrication mechanisms. η is lubricant viscosity, υ is sliding velocity, ρ is normal pressure and μ is coefficient of friction, modified from [42].

The contact condition in the cold pilgering process is mainly placed in the mixed lubrication region that is the mixture of boundary lubrication on the asperities and the thick film in unconnected valleys of the surface topology [16]. This contact condition is desired as the asperities can be flattened out and a smooth and shiny tube surface can be achieved. The oil thickness must not be too thin nor too thick. The latter result in a high amount of asperities that increases the risk for surface cracks. Too thin lubricant, on the other hand, increases the friction coefficient and causes accumulation of tube material on the tool. Built-up material on the tool damages the tube and shortens the tool life [16].

In this mixed lubrication region, the friction is determined by the composition of influences from the asperities and the lubricant behavior [45]. The lubricant behavior is mainly

influenced by the viscosity, contact pressure, relative siding speed and film thickness whereas the concentration of the asperities of work piece and tools influences the real contact area. The contact conditions vary much in the pilgering process. Large compressive stresses exist at the groove bottom and then asperity peaks are flattened out. On the other hand, this flattening is very low in the shoulder parts. The surface roughness of the tube surfaces varies not only within a given tool but also from tool to tool based on how many times they have been used. Additionally, chemical interaction between the lubricant and the tube and tool material is another factor influencing the surface properties [2].

The dominant factors determining the lubrication are oil film thickness, surface roughness, viscosity, relative sliding and contact pressure. Abe *et al.* [21] calculated oil film thicknesses over the working section in the cold pilgering process for different temperature, oil viscosity, tool design and feed and stroke rates. They showed how the oil thickness changes over the working section and also evaluated the influence of different oil temperatures, viscosities, tool design and process parameters. They showed that the viscosity vary with temperature and pressure. A particularly problem is that the viscosity decreases with temperature and then the cooling also becomes less effective. Thus the pilgering process exhibits very intricate friction conditions and standard test methods, such as ring compression test [34,41], are not sufficient to estimate the friction coefficients in cold pilgering.

There are no published full-scale experiments where the friction coefficient in cold pilgering has been estimated. Aubin *et. al.* [30] only concluded the friction coefficient on tube-roll surface is always smaller then tube-mandrel surface based on their full-scale experiments. Even though lab-scale experiments cannot fully represent the friction condition in the processes, they are employed to investigate the influence of lubricant on the friction. Hardell *et al*. [36,38] used cylinder-on-disk configuration and a sliding four-ball test for such investigation. They concluded that cylinder-on-disk method is suitable in ranking the performance of cold pilgering lubricants. In this test friction coefficient estimated between 0.2-0.3.

2.6 Process temperature

As described earlier, a large amount of heat is generated during the process and is transferred to the preform, rolls and mandrel. It is removed by convection to surrounding and most important by the lubricant. The heat on the preform and groove surfaces is progressively dissipated by lubricant, see Figure 14. However, it is difficult for the heat to dissipate from the inner surface of the preform and the mandrel due to low lubricant flow. For some process conditions the heating can cause temperatures on inner and outer surface of the cone up to critical temperatures, 250-300°C, where the lubricant gets burnt. Temperature increase also

influences the oil film thickness, hence the friction, shown by Abe *et al.* [21].Thus controlling the process temperature is important.

There are several process and design parameters that influence the process temperature such as feed and stroke rates, lubricant flow, tool design etc. There is no investigation in the literature regarding the influence of the process conditions on the process temperature.

2.7 Rolling and reaction forces

Estimating the reaction forces in the process is important when designing the machine elements and tool. They have to stand the stresses as well as being sufficient stiff. Large forces on the mandrel and roll dies lower the life time of these tools and cause breakage. Moreover, increasing axial forces on the inlet chuck cause self-feeding problems. Even though there have been many published analytical formulas and FE models to calculate forces in the process, it is still complicated since so many factors affect it.

3 State of art in cold pilgering simulations

Several analytical models have been published in the literature to increase the understanding of forces and deformations in the cold pilgering process. They are used in the industry for the mandrel and groove design. The main advantage of these models is the simplicity of the models and they do not require expensive software licenses, as is the case for general FE codes. However, they are based on considerable simplifications and thus cannot reach the accuracy of FE models for a complex process such as cold pilgering.

3.1 Analytical models

The first attempts to model the forming process of cold pilgering were made by Siebel and Neumann in 1954 [46] and Geleji in 1955 [47]. These analytical models utilize a strip rolling analogy where a slab in the thickness direction is compressed between the rolls. Integrating over all slabs in contact gives the rolling force. The contact length is approximated as $L=R\cdot\Delta h$, where R is the roll diameter and Δh is the thickness reduction. The roll force is in the case of cold pilgering varying along the axial coordinate, z, as a function of projected contact length, L_d, see Eq. 8. In this Equation, k is the average normal stress over z, which depends on the friction and yield strength, and D is the diameter over working section.

$$F(z) = k(z)\cdot L_d(z)\cdot D(z) \tag{8}$$

Siebel and Neumann approximated the projected contact length according to Eq. 9, as two sub-sections shown in Figure 16. In the first sub-section, L_{d1}, the preform has contact with both mandrel and roll die, whereas in the second sub-section, L_{d2}, it is just in contact with the roll die where the wave is pushed forward. In this relation, m is the feed length, Ψ is the die contact angle, δ is the mandrel contact angle, S_0 is the initial cross-section area and S is the cross-section at z. The force is then estimated, given in Eq. 10, by this contact length where μ is the friction coefficient, t is the wall thickness and σ_0 is the yield strength.

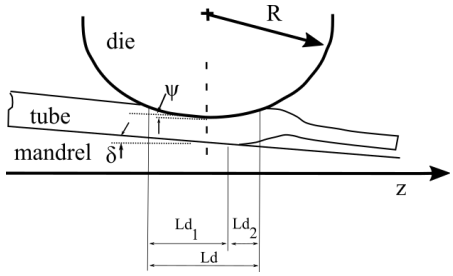

Figure 16: Longitudinal section of the contact area, modified from [31].

$$L_d = L_{d1} + L_{d2} = \sqrt{2R(z)m\left(\frac{S_0}{S(z)}\right)(\Psi(z) - \delta(z))} + \sqrt{2R(z)m\left(\frac{S_0}{S(z)}\right)\delta(z))} \tag{9}$$

$$F = \sigma_0(z)\left(\frac{1+\mu L_d}{2t(z)}\right)D(z)\sqrt{2R(z)m\left(\frac{S_0}{S(z)}\right)}\left(\sqrt{(\Psi(z) - \delta(z))} + \sqrt{\delta(z)}\frac{2t(z)}{D(z)}\right) \tag{10}$$

The models are based on the assumption of 2D axisymmetric conditions. They only consider the groove bottom and neglect the oval shape of the groove. Both of these models showed significant deviations in contact lengths, contact areas and rolling forces from the measurements by Yoshida *et al.* [23]. The differences were mainly attributed to the lack of tube turning in the formulas by the authors. Aubin *et al.* [30] claimed that the discrepancies were due to that the formulas do not account for the roll die flattening, existence of bulges and wave. However, all axisymmetric approaches ignore the asymmetric deformation of the process. It is described in Sec. 2.3 that contact length and rolling pressure vary significantly around the circumference.

Two decades later, Yoshida *et al*. [23] proposed a 3D simplified semi-analytical model of cold pilgering process using experimental measurements. They obtained the strain distribution, ε_θ, ε_r, ε_z, $\gamma_{z\theta}$, by measuring the material flow and thickness at each part of the surface of the gridded tube by stopping the processes at different instances. They assumed that the material flow is the same on the inside and outside of the preform. However, Aubin *et al.* [30] and Girard *et al.* [15] pointed out the importance of the shear strain, γ_{rz}, for damage evaluation. Yoshida *et al*. [23] found from measurements that axial elongation is always constant around the hoop direction. They estimated the normal Cauchy stress components from the measured strain components, neglecting shear. This information, together with known flow stress from experiments made it possible to compute the stress components assuming the stress state is on the yield surface of the material.

Another 3D model was developed by Furugen and Hayashi in 1984 [13]. They traced a feed element (hatched portion) from the preform to the finished tube in order to model the deformation history. Elongations after each stroke were estimated assuming plastic

incompressibility for the volume of the feed element. This is the first study where asymmetric deformation of the tube section and the elastic deflection of the roll stand were included in a pilgering model. They divided the tube cross section into four sections to include asymmetrical deformation trend of ovalised tube as shown in Figure 17.

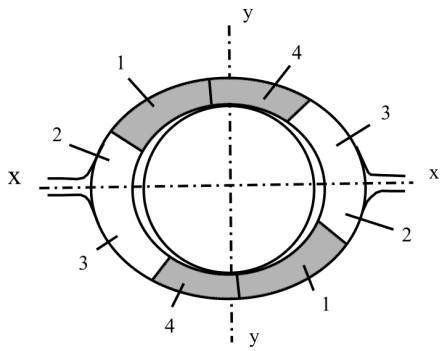

Figure 17: Partition of a tube-section, modified from [13].

The gap between the roll groove and mandrel is calculated by considering elastic deformation of the roll stand under the related rolling force. The mill modulus was experimentally calculated from the rolling force versus thickness variation between the roll dies. They estimated the Cauchy stress components in the same way as Yoshida *et al*. [23]. In 1992, Osika and Libura [48] developed a 2D and partly 3D mathematical model of cold pilgering to estimate the rolling pressure and axial force for the optimization of the tool shape (rolls and mandrel) but only considered one stroke. They stated that, without giving details, their model includes engine run irregularities and vibration of the drive system. This model employed the Neuman and Siebel formula to calculate the roll pressure. They expressed the 3D stress state as a combination of in-plane stresses over a transverse cross-section and uniaxial stress in longitudinal direction. Transverse cross-sections and the length of the tube were divided in smaller elements by using the matrix concept of FEM. Only one-fourth of the cross-sections were considered in the calculation by assuming symmetry in the cross-section.

Another important development was the analytical model by Fogelholm *et al.*[49] in 1991. This model is based on the axisymmetric assumption and divided the plastic zone of the work piece in 4 zones regions to compute incremental strains for each stroke. The sketch of the model is shown in Figure 18. The material is formed in Zone 1 and in contact with the mandrel. Zone 2 is the squeezing zone where the material has contact with both the mandrel and roll die. In Zone 3, the forging zone, the material has contact with only the roll die. In the last zone the roll die has not touched the material yet and it has no contact with mandrel either. The latter due to that they lost their contact in the previous feed step. In the sketch, V_k denotes the roll surface, R_k the caliber radius, R_d the mandrel radius and V_d the radius to the

inside of the material in the forge zone. L_{wk} represents the working length, L_f the feed distance and u the elongation during the stroke. Other variables z_v, z_p and z_q are the longitudinal coordinates at the boundaries between the zones. Elongations were estimated iteratively by assuming constant volume and homogeneous deformation.

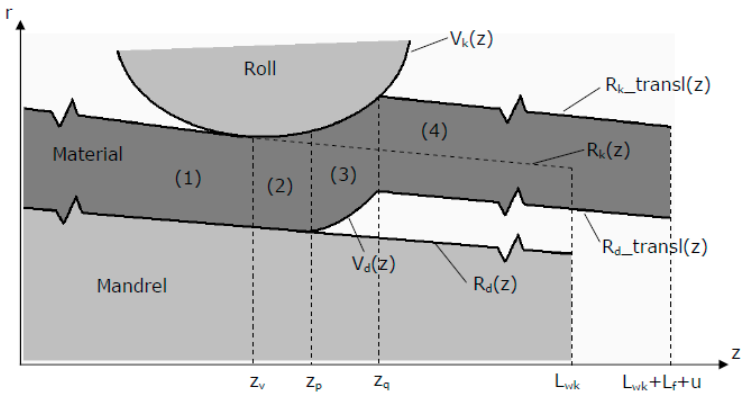

Figure 18: Sketch of the model by Fogelholm *et al.* [49].

The accumulated effective strain is then computed by Eq.s 11-14 as a function of the axial position and number of stroke.

$$\varepsilon(z_k)=\varepsilon(z_{k-1})+\Delta\varepsilon_{Shear}+\Delta\varepsilon_{Squeeze}+\Delta\varepsilon_{Forge} \tag{11}$$

Where

$$\Delta\varepsilon_{Shear}=\sqrt{\frac{1}{3}}\left(\arctan\left(\frac{dV_k(z_q)}{dz}\right)-\arctan\left(\frac{dR_k(z_q-L_f-u(z_v))}{dz}\right)\right) \tag{12}$$

$$\Delta\varepsilon_{Squeeze}=\sqrt{\frac{2}{3}(\varepsilon_r^2+\varepsilon_\theta^2)} \tag{13}$$

$$\Delta\varepsilon_{Forge}=\sqrt{\frac{2}{3}(\varepsilon_r^2+\varepsilon_\theta^2+\varepsilon_\theta^2)} \tag{14}$$

The principle strains, ε_r, ε_θ, ε_z, have different signs in the squeezing and forging zones as given in Table 2.

Table 2: Principle strains.

Squeezing	Forging
$\varepsilon_r>0$	$\varepsilon_r<0$
$\varepsilon_\theta>0$	$\varepsilon_\theta>0$
$\varepsilon_z>0$	$\varepsilon_z>0$

These strain increments were used to estimate stresses required in the plasticity calculations. The flow stress model accounts for the strain softening and temperature dependence. This model was the first model including these phenomena. A one dimensional and time averaged temperature profile is used in the thermal model and calculated at a discrete set of points along the length with some simplifications, described in Sec. 3.4. Finally, the rolling force is calculated using the slab elements method according to Eq.15, where L_k is the contact length and m is the friction factor. This relation is only applied in the forging zone and ovalisation is neglected. Relative sliding of the roll/cone interface is also neglected.

$$F = 2\sigma(z)R_k(z)L_k\left(1+L_k\frac{m}{2}\frac{(R_k+R_d)}{(R_k^2-R_d^2)}\right) \tag{15}$$

Osika and Libura [50] created 2D and 3D analytical models to investigate the optimum tool shape. They simulated one stroke of the process to examine the rolling pressure and the axial force.

Aubin *et al.* [30] developed a 3D semi-analytic model, which was another pioneering attempt due to including some important phenomena as the first time in a model of cold pilgering. They considered elastic tool deflections, and the roll flattening using Hitchcock's formula [51] and wave. The model is based on the slab method [52-54] and experimental measurements. The model first calculates the geometric evolution of the tube with the basic idea of Hayasi *et al.* [13]. The axial displacements of a material point during strokes are estimated. Later, corresponding diameters and cross-sections at the related axial point are calculated based on the tool design where measured roll die gap, denoted *G* in Figure 19, used which includes the elastic deflections of the roll stand.

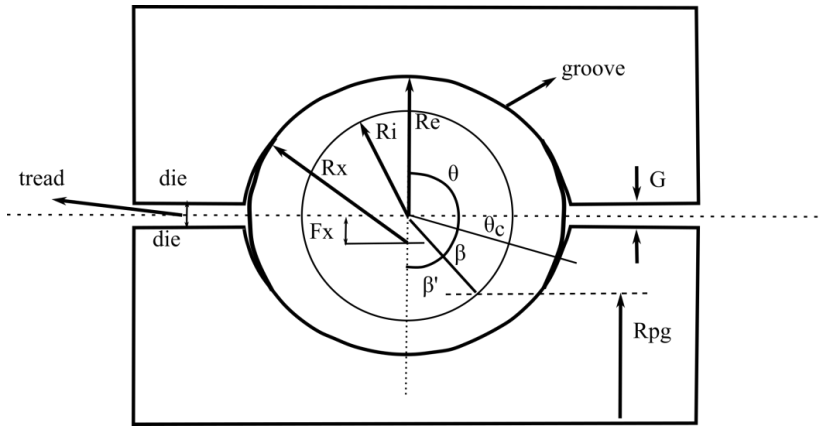

Figure 19: Cross section of the tube/mandrel/roll groove system, modified from [30].

This calculation of the motion is used to compute the elongation and diameter evolution giving incremental strain components, $\Delta\varepsilon_{rr}$, $\Delta\varepsilon_{\theta\theta}$, $\Delta\varepsilon_{zz}$, by Eq.s 16-18. In these equations S and D represent the cross section area and the average diameter respectively after the stroke, n.

$$\Delta\varepsilon_{zz}=ln\left(\frac{S_{n-1}}{S_n}\right) \tag{16}$$

$$\Delta\varepsilon_{\theta\theta}=-ln\left(\frac{D_{n-1}}{D_n}\right) \tag{17}$$

$$\Delta\varepsilon_{rr}=-\Delta\varepsilon_{zz}-\Delta\varepsilon_{\theta\theta} \tag{18}$$

They measured the torsional and shear strains, ε_{rz} and $\varepsilon_{\theta z}$, by using a special preform with drilled holes, and used them in the model as it is too difficult to calculate them. They stated that the torsional strain is negligible (0.02-0.03) and calculated the shear strain by Eq. 19 where β', β and θ_c are design parameters given in Figure 19. The strain component, $\varepsilon_{\theta r}$, was not mentioned in their work.

$$\Delta\varepsilon_{rz}=\varepsilon_{rz}\frac{\Delta\varepsilon_{zz}}{\varepsilon_{zz}}\left(\beta'-(\beta-\theta_c)\right) \tag{19}$$

The stress components are estimated in Eq. 20-22 from the strain increments and by employing the flow rule.

$$\sigma_{\theta\theta}-\sigma_{zz}=\frac{2}{3}\frac{\dot{\varepsilon}_{\theta\theta}-\dot{\varepsilon}_{zz}}{\dot{\bar{\varepsilon}}}\sigma_0=\sqrt{\frac{2}{3}}\frac{\Delta\varepsilon_{\theta\theta}-\Delta\varepsilon_{zz}}{\sqrt{\Delta\varepsilon_{rr}{}^2+\Delta\varepsilon_{\theta\theta}{}^2+\Delta\varepsilon_{zz}{}^2+2\Delta\varepsilon_{rz}{}^2}}\sigma_0 \tag{20}$$

$$\sigma_{rr} - \sigma_{zz} = \frac{2}{3}\frac{\dot{\varepsilon}_{rr} - \dot{\varepsilon}_{zz}}{\dot{\bar{\varepsilon}}}\sigma_0 = \sqrt{\frac{2}{3}}\frac{\Delta\varepsilon_{rr} - \Delta\varepsilon_{zz}}{\sqrt{\Delta\varepsilon_{rr}{}^2 + \Delta\varepsilon_{\theta\theta}{}^2 + \Delta\varepsilon_{zz}{}^2 + 2\Delta\varepsilon_{rz}{}^2}}\sigma_0 \quad (21)$$

$$\sigma_{rz} = \frac{2}{3}\frac{\dot{\varepsilon}_{rz}}{\dot{\bar{\varepsilon}}}\sigma_0 = \sqrt{\frac{2}{3}}\frac{\Delta\varepsilon_{rz}}{\sqrt{\Delta\varepsilon_{rr}{}^2 + \Delta\varepsilon_{\theta\theta}{}^2 + \Delta\varepsilon_{zz}{}^2 + 2\Delta\varepsilon_{rz}{}^2}}\sigma_0 \quad (22)$$

In these equations the average value of σ_{zz} along the contact length was calculated by the slab method. The contact length was estimated by the modified version of Siebel and Neumann's formula, given in Eq. 23.

$$L_d = \sqrt{2R'(z)m\left(\frac{S_0}{S(z)}\right)(\Psi(z) - \delta(z))} + w\sqrt{2R(z)m\left(\frac{S_0}{S(z)}\right)\delta(z))} \quad (23)$$

The roll radius, R in Eq. 9, was replaced by the flattened roll radius, R', as estimated by Hitchcock's formula [51] in Eq. 24

$$R' = R\left(1 + \frac{16(1-\nu^2)}{\pi E}\frac{F}{\Delta h}\right) \quad (24)$$

where F is the rolling force E is the Young's modulus and Δh is tube thickness reduction during one stroke. Additionally, a fitting factor, w, for the wave was introduced in the model to calibrate the contact length, L_2, so that it increases the contact due to the wave in front of the roll. This calibration was made by fitting the measured contact length to the model, see Figure 20.

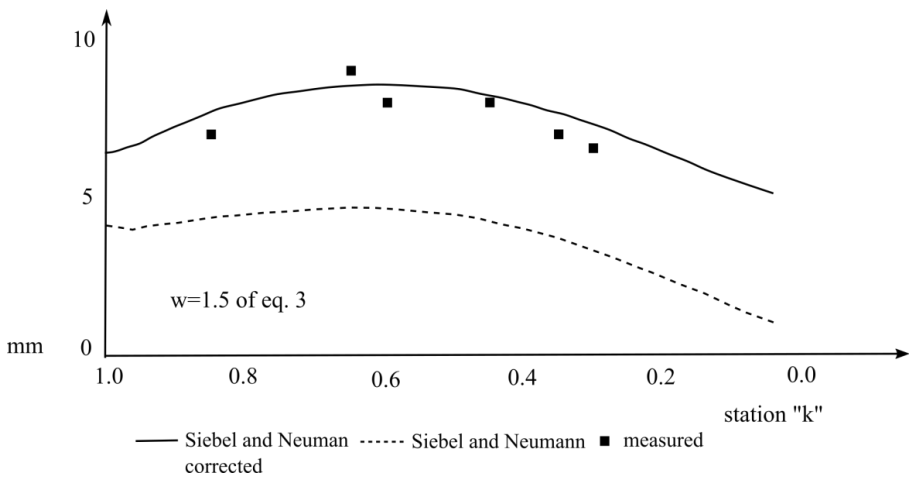

Figure 20: Comparison of experimental contact length L_d with theory [30].

Finally, the rolling force was estimated by integrating the vertical projection of the radial stresses, σ_{rr}, over the contact surface where the contribution from the axial components and friction stress are neglected. They showed that experimental rolling forces are in good agreements with the model. The axial force is similarly estimated by integrating the axial stress, σ_{zz}, over the cross-sections at the beginning of the contact. This could not validate due to experimental difficulties to measure axial forces separately. In 2000, the same author further developed the recent model to predict the shear strain, ε_{rz} [55].

The models have been developed from analytic to analytic-numerical (semi-analytic) in order to account for more of the complexities and further improvements (next section) of modeling requires more general numerical tools.

3.2 Finite Element models

3.2.1 Two dimensional models

Two-dimensional FE models of cold pilgering are often based on assuming axisymmetric conditions in order to decrease the computational cost. However, the deformation in cold pilgering process is not axisymmetric. Therefore, these models often underestimate the contact length and overestimate the roll force [23]. Moreover, the strain history can thus not be fully captured. This history is an important factor in cold pilgering since as it influences the hardening process, redundant work [2] and process temperature. However, these 2D models can be useful for qualitative evaluations, provided if one is aware of simplifications involved. For instance, Aubin *et. al.* [30] used this kind of model to investigate some local phenomena like the wave ahead of the rolls or shear strain, $\Delta\varepsilon_{rz}$. Their model indicated that the incremental shear strain, $\Delta\varepsilon_{rz}$, is proportional to the longitudinal strain increment, $\Delta\varepsilon_{zz}$. It was also found to depend on the friction coefficient and the sliding factor which is determined by tool design.

There are some published others in which 2D FE models were used for the investigation of cold pilgering. First of them is Davies *et al.* in 2002 [56] that they developed a 2D FE model. They used a 2D plane stress model to capture plastic strain distribution in the preform cross sections at four different working sections. The first two sections were located before and just after the preform has contact with the mandrel. The other two were at the middle and end of the working section. They found that this kind of models is useful for qualitatively investigate the direction and magnitude of the strain hardening.

Another study was published by Harada *et al.* [14] in 2005. They used a generalized plane strain model to investigate the tube spring-back. In this model, the tool was assumed to be rigid. However, the deflections of the roll stand were included in the model. They estimated

the roll stand stiffness as to 700 kN/mm by measuring the rolling force versus vertical roll movement. Moreover, the axial displacement of the mandrel due to elastic deflections is considered when the gap between the mandrel and rolls is set. To estimate contact length, they employed the modified version of Siebel and Neumann's formula similar to Aubin [30]. The modification accounts for the roll flattening and wave. The axial position of the work piece after each stroke was traced using feed length and reduction of cross-section area. The wave and roll flattening parameters were adjusted so that computed rolling force fitted the measured. They concluded that the spring-back effect of tubes must be accounted for when calculating the rolling force.

3.2.2 Three dimensional models

The first developed 3D mechanical FE model of cold pilgering was made by Mulot *et al*. [31]. They simulated one forward stroke for a partly pilgered preform geometry. They limited the model to the region of the preform that covers the mandrel, to decrease computational cost. They determined the initial geometry of the preform using coordinate measuring machine (CMM). This study was a pioneering work that, despite being limited to one stroke, showed the possibility to use of FE analysis for investigation of the cold pilgering process. They used rigid tools and neglected the deflections of the tool and roll stand. They compared their results with the semi-analytical model of Aubin *et al.* [30] and found that the strain increments over the working section differ in the different tangential position of the cross-section (bottom, flange and average). However, the reference semi-analytical model can only capture the averaged strain increment as it overestimates the rolling force. Their results show the propagation of a wave similar to the illustration in Figure 12.

This model was further extended by Montmitonnet *et al.* [29] in 2002 and three forward strokes were simulated, excluding the backward strokes. The initial geometry was predefined as in [31]. This means that the stress and strain histories were neglected. The FE code Forge3 was used in the simulations using an updated Lagrangian formulation. The tool was assumed to be rigid with and a penalty formulation was used for the contact between tool and tube. They proposed that, geometry and strain fields reach "pseudo-steady state" after two strokes for an ideal-plastic material.

Lodej *et al*. [57] used this model and created a post-processing procedure to determine the strain history of a material point that included work hardening. An equivalent strain field was estimated using Eq. 25, where S_0 is the initial tube section and S_z is the tube section along the partly pilgered tube, and initialized in the model..

$$\bar{\varepsilon}(z)=ln(\frac{S_0}{S_z}) \tag{25}$$

They simulated pilgering cycles with this initial state until the geometry and strain fields reach the "pseudo-steady state" after four cycles. They claimed that all other variables, geometry, strain and stress tensors converged similarly. Then the variation of the axial stress over the working section was determined. A post-processing procedure was applied at the "pseudo-steady state" integrating the single stroke displacements and rigid body movements of a material point. This process was iterated until the selected point from the preform reaches the end of forming zone. By this way they could determine trajectories of any material point, hence the full deformation histories.

Nakanishi *et al.* [35] developed 3D mechanical FE model of cold pilgering and computed the displacement field of the tube ends and mandrel. The explicit FE code LS-Dyna was employed for these calculations. The initial preform geometry was created using the gap between the mandrel/groove surfaces, means stress and strain history neglected. Tools, mandrel and rolls, were assumed rigid and supported with springs. The spring stiffnesses are $k_{roll}=3x10^{9}\frac{N}{m}$,$k_{mandrel}=38x10^{6}\frac{N}{m}$. The displacement of the preform is included using nonlinear spring with elastic spring constant, $k_{tube\_el}=4.75x10^{6}\frac{N}{m}$, plastic spring constant, $k_{tube\_pl}=23.75x10^{3}\frac{N}{m}$, and yield force of 600N.

Osika *et al.* [50] set up a physical lab-scale model of the process for cold pilgering of aluminum tubes. A square grid was etched on the tube before pilgering and the coordinates of the grid were measured to calculate the displacements after each stroke using a photogrammetry method. Later FEM and Finite difference method (FDM) were employed to calculate the strain fields. However, the inner surface of the tube was not included in the calculation so a full 3D strain field could not be obtained. This physical model was further improved in a following study by Pociecha *et al.* [58]. They inserted copper sticks into the aluminum tube to make it more visible when measuring. They then assumed plane cross-sections and calculated the total strain using Eq. 26 where S_0 is the initial cross-section and S_1 is the final cross-section.

$$\varepsilon=\frac{S_0}{S_1} \tag{26}$$

They used the FE code Abaqus in their simulations and assumed rigid tools. An explicit time stepping method was used and the density was scaled to reduce the calculation time.

3.3 Friction modeling

Friction properties are difficult to obtain but important when modeling metal forming processes [59]. There are two commonly used models, Coulomb and Tresca. The friction force increases linearly with increasing contact pressure in the Coulomb model, see Eq. 27,

where μ is the friction coefficient, p is the normal pressure and τ_f is the frictional shear in the direction of the relative motion of the contacting surface. However, the yield stress of the material limits the increase in the shear stress, hence the friction force. Therefore, there is a natural limitation to the friction shear stress in this model. However, sometimes there may be an interface oxide layer that is not accounted for in the flow stress model of the bulk material. If this is the case and this layer breaks up and lubricates the surface at a stress level below the natural limit due to bulk plasticity, then one adds a cap on the Coulomb model as indicated in the curved line in Figure 21 or as in Figure 22.

$$\tau_f = \mu p \tag{27}$$

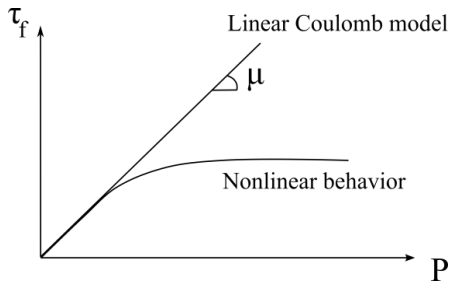

Figure 21: Shear force vs contact pressure relation [60].

The Tresca model gives a constant shear stress, τ_f, proportional to the yield limit in shear, denoted k, according to Eq. 28.

$$\tau_f = mk \ , \quad 0 \leq m \leq 1 \tag{28}$$

There is no relative sliding when the shear stress is below τ_f. These two models can be combined as shown in Figure 22. The Coulomb model is then limited by the Tresca model at the high contact pressures. Then there is always some relative sliding between the surfaces in contact.

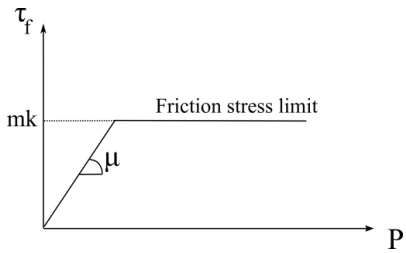

Figure 12: Mixed friction model.

All models are very simplified when considering the complexity of the friction conditions in the real process as discussed in Sec 2.5. There are more somewhat more advanced models in

literature like Wanheim and Bay's model [61] and Bowden and Tabol's model [62]. There are also FEM investigations for mixed lubrication friction [45,63]. However, the real problem is not the choice of model but acquiring the needed parameters. The Coulomb and Tresca models are commonly used in publications with cold pilgering models. The friction coefficients vary in these publications between 0.03-0.2.

3.4 Temperature model

There is only one published analytical model for estimating the process temperature in cold pilgering [49]. It gives a one dimensional and time averaged temperature profile at a discrete set of points along the length of the tube. It is assumed that the tube inner wall and the mandrel have good thermal contact and the temperature is assumed to be constant in the radial direction. Thus, the mandrel and tube wall are modeled as a single thermal system. The cooling by lubricant over the outer surface is included. The thermal conductivities of the tool and the tube are assumed to be independent of temperature. Heat generation due to the friction between the rolls and the tube is neglected. This model also considers the heat flow during the transport of material (feeding) along the mandrel due to temperature difference between neighboring sections. The heat is calculated according to Eq. 29 at discrete sections along the axial direction. It is the sum of heats due to the plastic deformation (Q_{def}), the friction between the mandrel and tube (Q_{fric}), cooling of the tube by the oil ($Q_{oil\text{-}tube}$), conducted heat between neighboring sections ($Q_{tube\text{-}sec}$) and the heat flow due to the transfer of the tube material along the mandrel ($Q_{mat\text{-}trans}$). The temperature distribution along the working section is then calculated by solving the energy balance equations for each section.

$$Q_{def}+Q_{fric}+Q_{mat\text{-}trans}=Q_{oil\text{-}tube}+Q_{tube\text{-}sec} \tag{29}$$

3.5 Constitutive modeling

Employing a reliable constitutive model, which can predict strain hardening, is important in the modeling process. The strain field in cold pilgering is very complicated due to the non-proportional multi-axial loading-unloading history. Hardening and recovery processes occur simultaneously during the deformation and in a very complex way in during the process. Armstrong *et al*. [64] performed series of multidirectional cyclic compression tests with aluminum cubes at room temperature in three different orthogonal directions. Results showed the saturation stress depends on the strain increments, see Figure 23. Similar observations were documented in literature for other metals. In addition, temperature and strain rate varies along the working section and circumferential direction. Influences of temperature and strain rate on the flow stress are well known phenomenon [65].

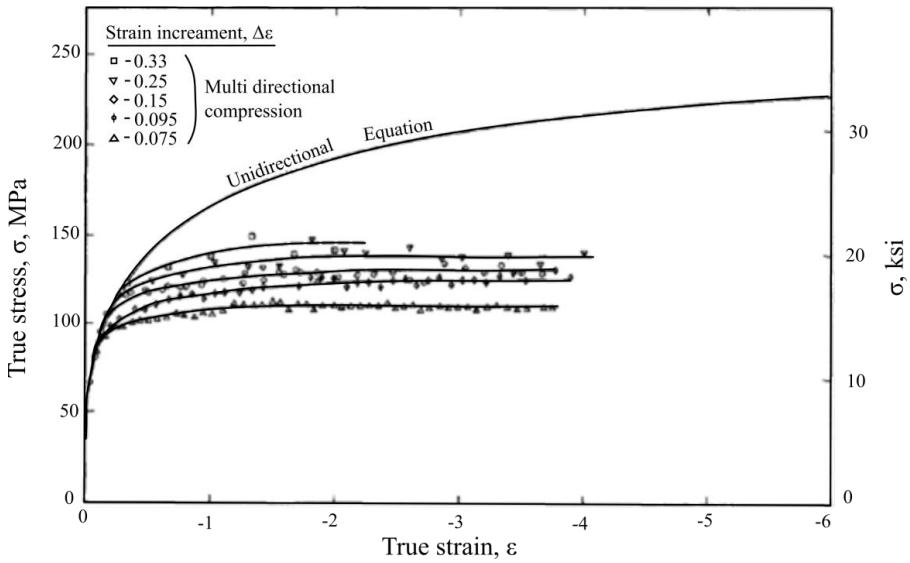

Figure 23: Summary of multidirectional compression tests on annealed 1100 aluminum [64].

There are a large number of constitutive models in the literature categorized in two main groups. First of them is crystal plasticity models that can predict texture evolution and thereby anisotropic evolution. Several investigations have been made with these models for studying phenomena in the cold pilgering process [15,66-69]. They can be only applied for small volumes, as the different slip planes in the crystal must be resolved. The other possibility is macroscopic scale models. The framework of this work covers macro scale investigations by plasticity models. Yield surface plasticity is used to predict the inelastic response of metals to the related loading. These models consist of a criterion for yielding, a plastic flow rule and a hardening rule [70]. The yield surface evolves during the hardening based on the history of plastic deformation. The assumption of isotropic hardening makes the yield surface grow but not change shape and neither move in stress space. Another extreme case is to assume pure kinematic hardening. Then the shape and size of the yield surface is maintained but it moves in stress space due to back-stresses in the material. None of these approaches accounts for texture evolution that makes the shape of the yield surface change.

Davies *et. al* [56] experimentally investigated the yield surface evolution during cold pilgering of titanium alloy tubing using biaxial testing. For this metal, they concluded that anisotropic Hill's model [71] fit the experimental yield surface better than isotropic von Mises criterion. Vanegas-Márquezes [72] used anisotropic Hill's model in a FE simulation of the HPTR cold pilgering of ODS steels. The model was calibrated versus tests on specimens cut out from extruded rods of ODS steel instead of preforms. They concluded that using the

anisotropic model improves the stress and strain prediction compared to an isotropic model. They also pointed that using tubes instead of rods for tests can lead better results in the identification of the parameters of the Hill's model.

Vanegas-Márquezes *et. al* [32] used a simple approach based on Chaboche model [32] which includes both kinematic and isotropic hardening variables to investigate hardening of an ODS steel in pilgering conditions. This model contains rather fewer parameters (10 parameters). To calibrate the model parameters, they did both tension-compression and compression-compression test cycles. They concluded that compression-compression test cycles are more suitable to capture and model the hardening trend in cold pilgering. Vanegas-Márquezes [72] showed that in HPTR cold pilgering this approach can capture the flow stress better compare to isotropic and anisotropic monotonic models. Sornin *et al.* [73] implemented this model in FE model of HPTR cold pilgering in MSC. Marc.

Most publications of FE models of the VMR cold pilgering processes use simple 1D isotropic hardening using either phenomenological models [14,55,57,74,75] or tabulated flow stress data [13,35]. However, these models tend to overestimate stress values, therefore rolling force, as they lack kinematic hardening [28,72,76]. Huml *et al.* [77,78] used more advance formula in their analytical model for flow stress, which includes parameters to consider the influence of temperature, strain rate and softening due to cyclic multi-directional deformation.

4 Developed cold pilgering simulation

This chapter describe the development of the numerical cold pilgering model in the course of this thesis work. **Paper I- IV** are preliminary studies where different phenomena in modelling process were investigated and new features were added in order to improve prediction capability. **Paper V** and **paper VI** are based on the final versions of the material model and process model, respectively.

A simplified 3D thermo-mechanical FE model of cold pilgering was developed in **paper I**. The influence of temperature on the rolling force was investigated in this study. The Johnson-Cook model was employed to describe the flow stress assuming isotropic hardening. The results suggested that temperature have a significant influence on the roll force as shown in Figure 24, therefore it should be included in the modelling process.

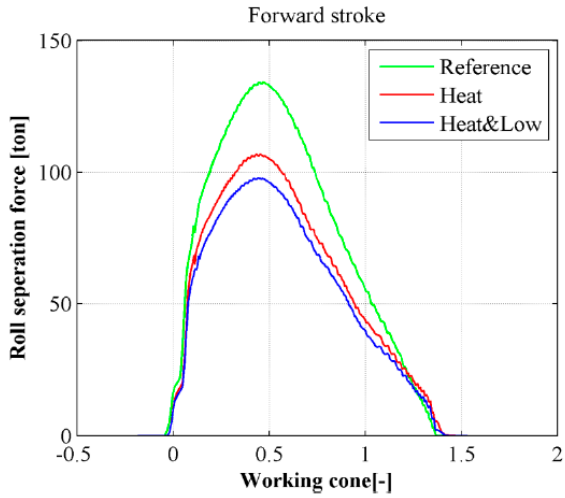

Figure 24: Rolling force over the pilgering strokes, the red and green lines indicate calculations with temperature dependent and independent material model.

However, it was also observed that Johnson-Cook model that is calibrated using tensile test is caused a too large rolling force. This problem occurs when accumulated plastic strain becomes large as shown in Figure 25. This is due to the fact that this material model is not capable of capturing strain recovery leading to a reduced hardening at large strains. This observation suggested the use of a material model that can include strain recovery.

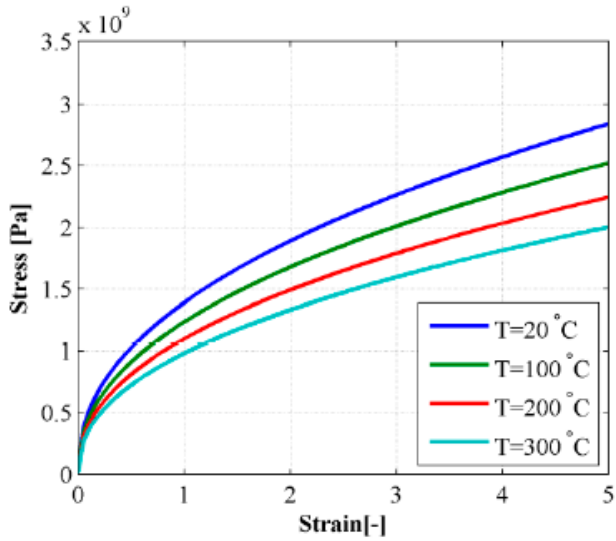

Figure 25: Stress-strain curve calculated by Johnson-Cook model at various temperatures.

The aim in **paper II** was to investigate the influence of elastic deflections of the tools on the rolling force and accumulated plastic strain. To prevent the overestimation issue in **paper I**, a tabulated flow stress curve with an upper limit of the flow stress for large strains was used. Elastic deflections in horizontal direction in the mandrel and preform occur because of the forces on the long preform and mandrel rod that are connected to the mandrel. Deflections in the vertical direction of the rolls occur due to elastic deformation of the roll stand. In the FE model, mandrel, tube and rolls were supported with elastic springs, as shown in Figure 26, to capture these deflections.

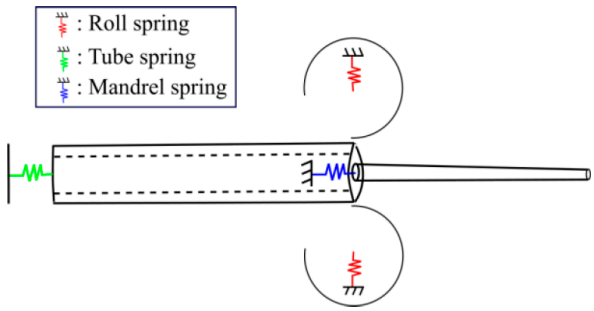

Figure 26: Inserted springs to mimic deflections of tools.

A parametric study was performed to investigate the effect of the spring stiffness on the strain path and the rolling force. It was shown that the stiffness of the tube preform has a significant impact on the roll force during the backward stroke. Moreover, including the springs changes the rolling significantly. Figure 27 shows their influence. This findings study suggested that the elastic deflections of tube and rolls should be included in the model to reach reliable force prediction.

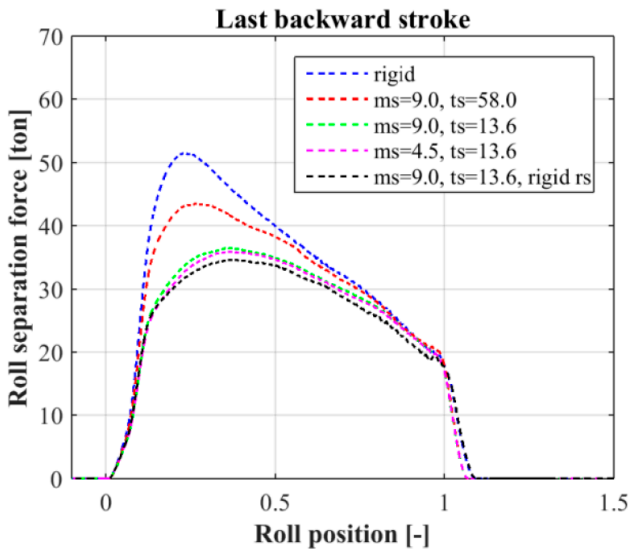

Figure 27: Rolling force vs roll position during the backward position. Blue line is the case with no flexibility. Red and green lines are the cases with large and small spring stiffness in tube, representing long and shot preforms.

This model was extended in **paper III** with elastic roll dies. The influences of roll die deformation on the contact region, roll force and tube dimensions were investigated. Re-meshing is utilized in order to better capture the difference in the contact length and tube dimensions between the models with rigid and elastic roll dies accurately. Figure 28 shows the contact region in the FE model.

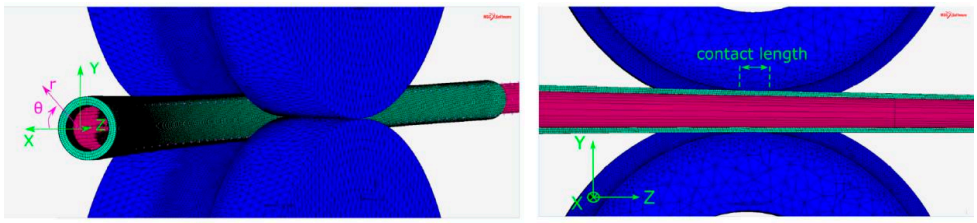

Figure 28: A section of the contact region in the FE model.

Full-scale experiments were performed to validate the contact surface and tube dimensions. Figure 29 shows the borders of the contact surface between the partly formed tube and roll dies in experiments and the FE model.

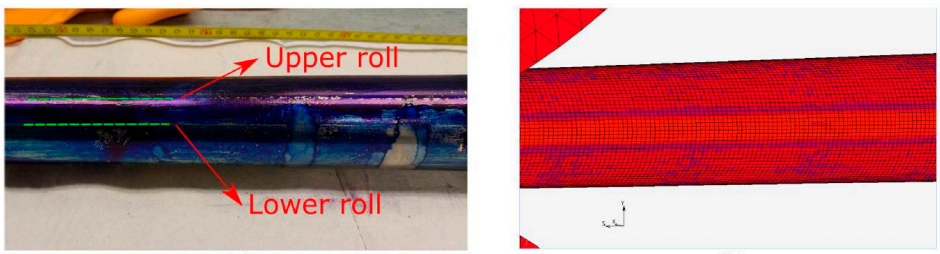

(a) (b)

Figure 29: The borders of the contact surface between the partly formed tube and roll dies in **a)** experiments and **b)** the FE model.

Results showed that the influence of roll die flattening in cold pilgering is of minor importance when predicting contact length. On the other hand, the roll die deformation has around 5% influences on the roll force. Therefore, using elastic roll dies in the simulation increases the accuracy of the calculation somewhat. However, using elastic roll dies in the simulation adds very large amount of calculation time and computational cost. Since there is no noticeable difference in contact length between an elastic or rigid roll die, then it is sufficient to include elastic deformations via springs attached to rigid roll dies to save computational time.

The focus in **paper IV** was on understanding hardening/softening behaviour of the material when the loading direction changes which we experience in cold pilgering. The influence of alternating loading directions on work hardening was experimentally investigated for 316L stainless steel. A cyclic plasticity model based on Chaboche-type approach with single set of parameters was tested to see if this model is capable of mimicking work hardening under alternating loading directions. A simplified fitting method was used to identify the parameters. Optimized model showed overall reasonable agreement. However, it was noted that single set of parameters in the Chaboche model was not fully capable of capturing work hardening over the whole region of large accumulated strains. Dominant mechanisms that control the work hardening may change due to the very large accumulated plastic strains.

This study suggested that Chaboche type of plasticity model in general is suitable to mimic hardening behaviour in cold pilgering. It could capture stress saturation at large accumulated plastic strain, therefore did not cause overestimation like in Johnson-cook model. Also, it could follow the hardening trend. However, it can simply be improved by adding another set of parameters for large strains.

Paper V further focused on the compression-compression test in alternating directions. The model in paper IV was extended with Chaboche parameters that depend on accumulated plastic strain. An optimization algorithm was developed to identify the model parameters. The cyclic compression-compression test and monotonic tensile test results with the samples from the tube preform were compared. Figure 30 shows the influence of loading path on strain hardening by comparing cyclic and monotonic test. This finding indicates that extending a monotonic tensile to large strains overestimate the stress around 15% for cold pilgering compared with the Chaboche model.

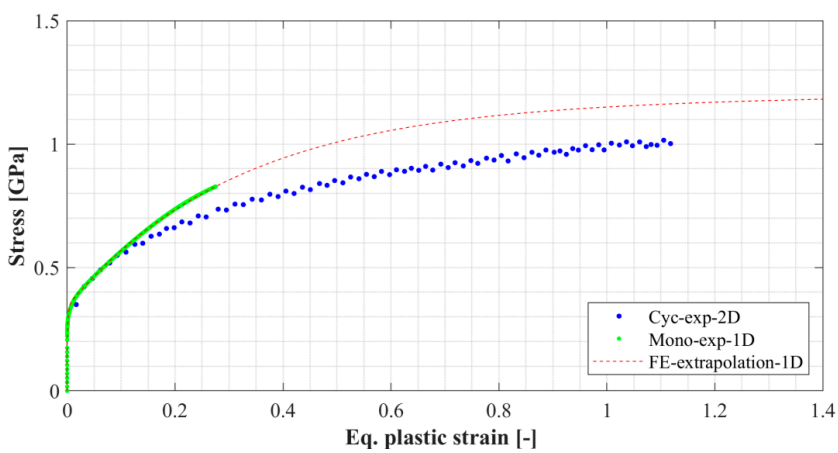

Figure 30: Compression-compression test vs. monotonic tensile test.

The Chaboche model parameters depend also on temperature in addition to the dependency on equivalent plastic strain. This modification significantly improves the fit versus experimental values for 316L for the large strain region during alternating compression tests. The constitutive model is implemented in a Matlab™ routine. The equations are solved using a fully implicit backward Euler return mapping method. This routine was used in an optimization algorithm based on nonlinear least-square solver to identify the model parameters by using experimental compression-compression test and tensile test. The optimized parameters of Chaboche model are functions of equivalent plastic strain and temperature. They were implemented in the 3D thermo-mechanical FE model of cold pilgering. Computed yield stress at room temperature in the transition zone (working section), from preform until the final tube, is given in Figure 31. This computed results later compared with hardness test that was performed at transverse sections of the partly formed cone of 316L and hardening trends showed good agreement. In addition, experimental and computed stress-strain curves on samples taken from the final pilgered tube are compared under tensile loading at three different temperatures and a close agreement was found. The comparison is given in Figure 32. It is validating the influence of the deformation history on the final material properties. One conclusion from these results is that the material model is sufficient accurate to be used for simulating cold pilgering.

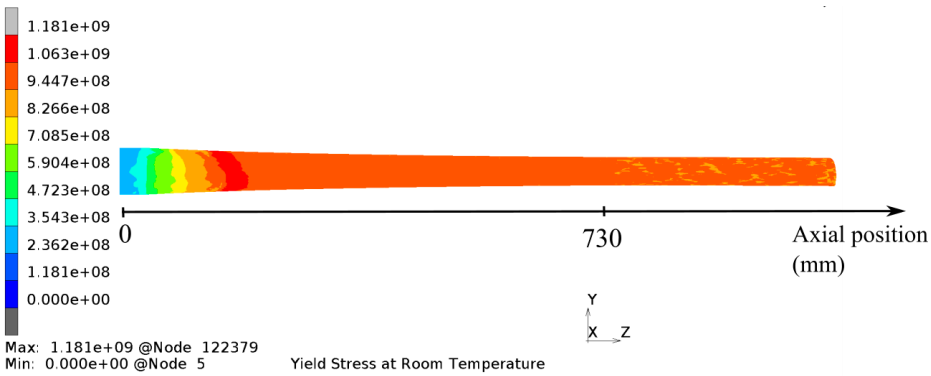

Figure 31: Yield stress distribution at room temperature calculated by FEM.

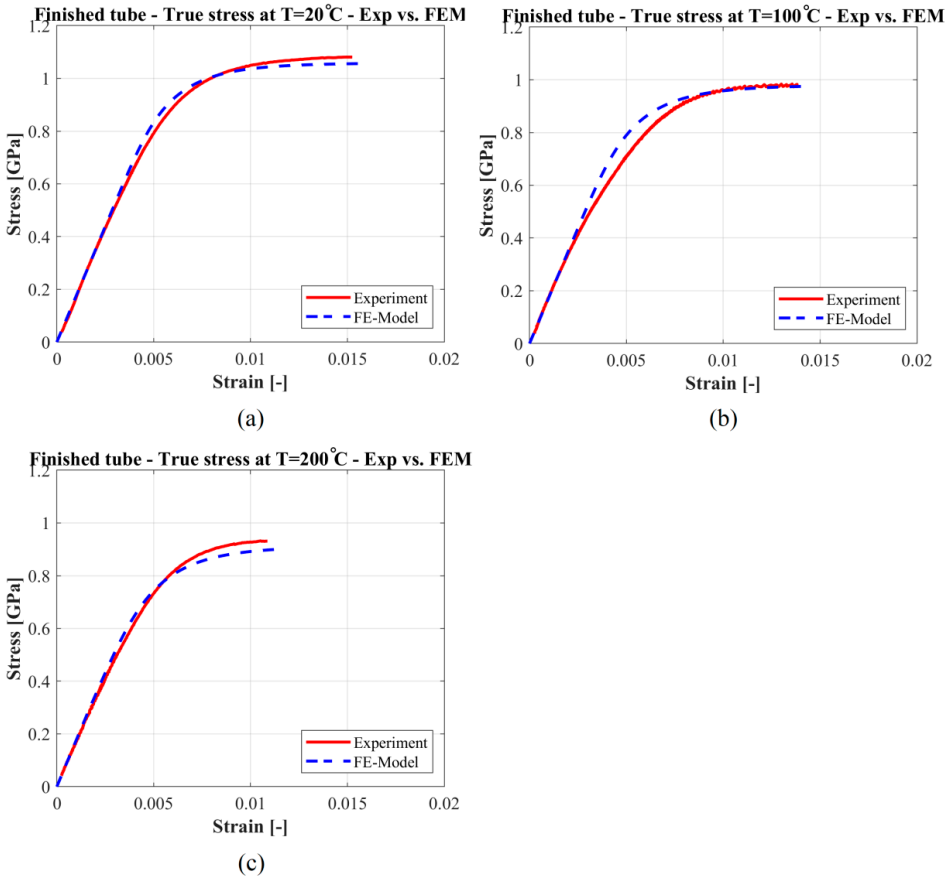

Figure 32: Flow stress in final tube from experiment vs FEM prediction at RT, 100 °C and 200 °C.

The model in P**aper VI** combines all previous developments. The temperature, and strain range dependent cyclic plasticity model, was taken from **Paper V**.

P**aper VI** presents a validated thermo-mechanical three-dimensional (3D) Finite Element (FE) model of cold pilgering. It can predict geometric evolution, rolling force, process temperature and deformation hardening. The experimental methods consist of both material characterization as well as process measurements.

Full-scale trials were performed in the production to calibrate thermal and mechanical parameters in the FE model and validate the model. Tool deflections are included in the

model by nonlinear springs that were calibrated by means of measurements. Roll die deflections during pilgering strokes were measured to validate the model. Temperature changes inside mandrel and on workpiece were also measured to calibrate thermal parameters and validate calculations. Figure 33 shows the comparison of FE prediction with calibrated thermal parameters vs experiment.

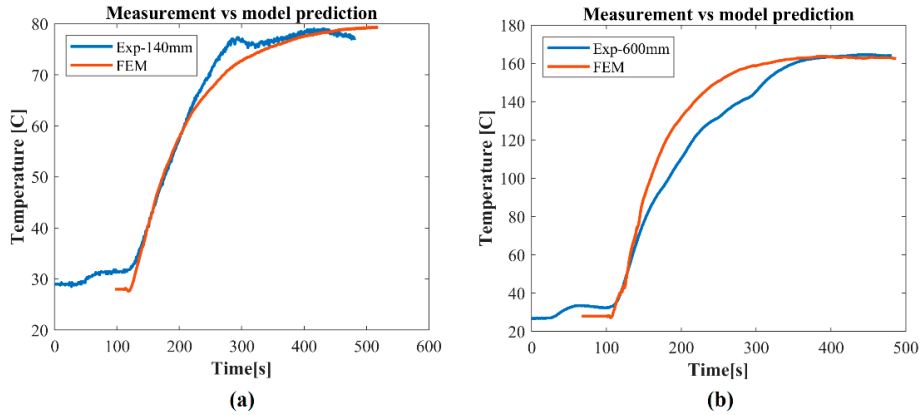

Figure 33: Temperature change inside the mandrel at 140 mm and 600 mm.

A partly formed preform was cut off from the process in a pilgering trial to measure geometric evolution using a Coordinate Measurement Machine (CMM). The CMM setup and an example of point cloud is shown in figure 34.

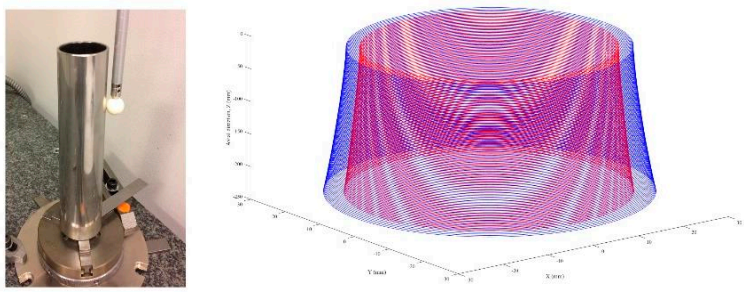

Figure 34: CMM measurement and point cloud from CMM measurement.

Geometric evolution in the FE model was compared with this measurement, see Figure 35, where the wall thickness variation along the working section is in good agreement with the

experiment. This data indicates that roll die and mandrel geometries together with deflections are represented accurately in the simulation.

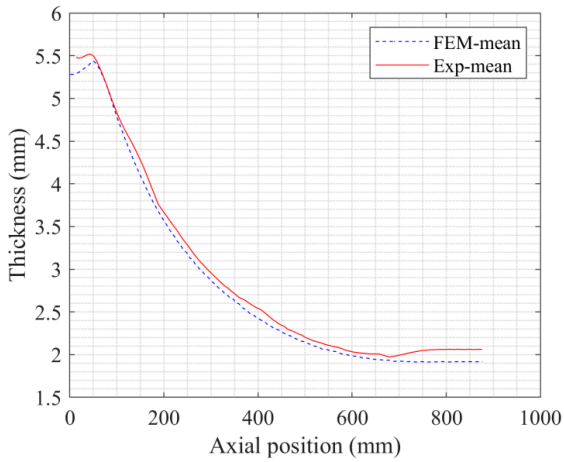

Figure 35: Mean wall thickness changes in the 3D FE simulation and experiments

Roll die deflections are used in this study to validate the rolling force indirectly since they are connected via the measured roll-stand stiffness. Computed vs experimental roll die displacements in the vertical directions are presented in Figure 36a and Figures 37 and 38. The agreement in this figure concludes that the chosen approaches for the FE and material models give a good prediction of the rolling force which is presented in Figure 36b.

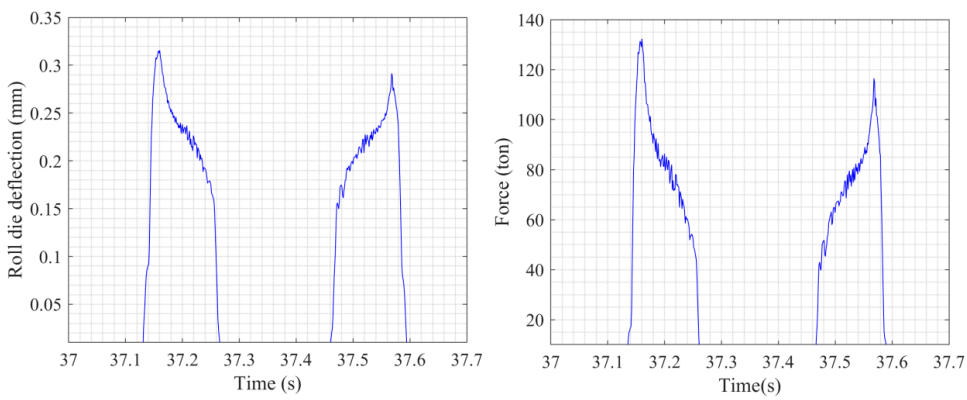

Figure 36: **a)** Roll-die deflections and **b)** rolling force calculated in the FE simulations of cold pilgering.

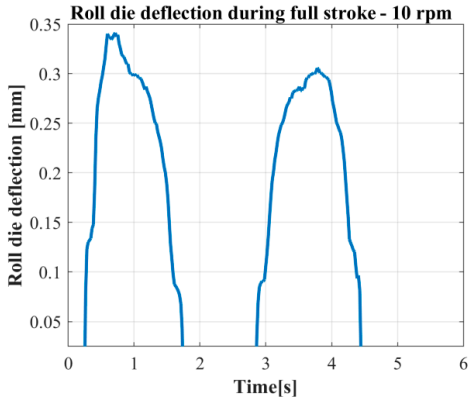

Figure 37: Upper roll die deflection during forward stroke and backward stroke at 10 rpm.

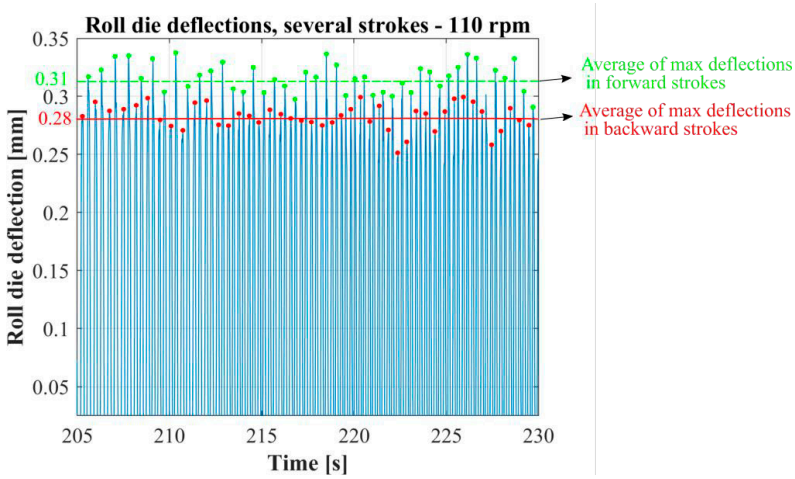

Figure 38: Upper roll die deflections, several strokes at 110 rpm. Green and red dots show max deflections in forward and backward strokes respectively.

5 Conclusions and future work

5.1 Conclusions

This work presents development of a validated thermo-mechanical three-dimensional (3D) Finite Element (FE) model of cold pilgering that can predict geometric evolution, rolling force, process temperature and deformation hardening. The focus was mainly on predicting those parameters since those are the most critical parameters that could limit productivity. Exceeding the rolling force limit could cause bearing failures, and damage roll dies and mandrel. Process temperature could limit outcome rate since extensive heat generation could burn oil and damage tube surface. Tube geometry is important when producing high precision tubes with tight geometric tolerances. In addition, mechanical properties are expected to be at certain level which depends on the product segment and application.

Some answer to the research questions (R1-4) in Ch 1.4 have been obtained. A number of improvements in modelling of cold pilgering have been found to be important (R1). They are listed below.

- Linear and nonlinear springs to capture elastic deflections of roll stand and preform
- Material model that can include both strain hardening and softening when material undergoes large multi-directional load history
- Temperature dependency dimension in material model to capture temperature effect on work hardening/softening
- Surface films for conductive heat exchange between lubricant, workpiece and mandrel to simulate process temperate.

The material model has also been improved in the course of this work (R2-3). A particular large improvement was obtained based on the experiments in [79] leading to a Chaboche type of plasticity model. These developments needed a number of measurements for calibration (R4). Finally, validation experiments are essential in order to state whether the main question "How should a sufficient accurate finite model of the cold pilgering process of tubes be formulated in order to be useful for design of the process?" has been answered. The validation experiments are

- Measurement of roll die deflections during pilgering strokes
- Hardness test on preform, partly formed tube and final tube sections
- Tensile tests on preform and final tube
- Dimensional measurement of partly formed tube sections in CMM
- Temperature measurement inside mandrel and on tube in working section

Temperature predictions are in close range with measurements. The deviation between calculation and measurements is in the range of 20-45 ˚C. This is acceptable when considering that material properties are not particularly sensitive to this deviation for the temperatures below 400 ˚C. The differences between measurements and computed roll-die deflections in vertical direction are less than 4-5% which is fairly good when considering the variations in the process. A safety factor of 10% in rolling force is normally used by operators and engineers when designing pilgering process to compensate uncertainties. The prediction by the 3D simulation is within that limit. Wall thickness (WT) and outer diameter (OD) calculations by the 3D simulation are within the tolerance that is 0.75% for OD and 10% for WT. Eccentricity ratio calculation on the other hand is not as good as OD and WT. Even if they are in same order of magnitude, there are 30-60% deviations. This needs to be further investigated. Lastly experimental and computed stress-strain curves in the final pilgered tube at room temperature, 100 ˚C and 200 ˚C are in good agreement. The deviations are limited with 50MPa which is nearly 4-5%. This deviation is within the tolerance which is in the range of 8% for the corresponding material and product.

Overall, reasonably close agreements were obtained in the comparisons. This result shows that the material modeling approach together with FE modeling approaches could successfully simulate temperature, rolling force, geometric variation, and flow stress of the final tube in cold pilgering process. The calculation time in the current simulation is around 4-5 weeks. Even though this is acceptable for research purpose or when exploring concepts, it is too long for use in design of the production process. This study showed the proof of concept, and the developed model can be used as a reference case to develop and calibrate simplified versions for industrial applications. The precision can still be improved and that suggestions are given in the next chapter.

5.2 Future work

In order to further improve the simulation of cold pilgering, the following subjects are recommended for future research.

- Eccentricity prediction in the simulation is not as good as other predictions. The reason of deviation is not fully understood. It could be further investigated.
- In this work isotropic yield surface was used. Anisotropic yield surface models such as Hill's model may further improve the stress predictions.
- Crystal plasticity models is getting increasingly popular for metal forming application to capture micro-structural changes. They can subject to the strain history at some selected points in the FE model obtain more information about the texture evolution.

References

[1] O Strehlau. Introducing cold pilger mill technology, TPJ-The Tube & Pipe Journal. 17 (2006) 32-33.

[2] HS Valberg, Applied metal forming: Including FEM analysis, Applied Metal Forming: Including FEM Analysis, 2010, pp. 1-465.

[3] K Brensing, B Sommer. Steel tube and pipe manufacturing processes, Salzgitter Mannersmann Rohrenwerke. (2008).

[4] G Stapleton, Cold Pilger Technology, Glen Stapleton 1996.

[5] Cold Pilger Mills, SMS MEER catalog, https://www.sms-group.com/.

[6] Sandvik Material Technology, Unpublished internal documents,.

[7] A Nerino, M Deaver, C Nagele, J Reinhart. HPTR'S PAST, PRESENT, AND FUTURE--PART I, TPJ-The Tube & Pipe Journal. 22 (2011) 16-21.

[8] S Hansson. Modeling of the Stainless Steel Tube Extrusion Process, (2010).

[9] Sandvik Material Technology, http://smt.sandvik.com/en/,.

[10] H Abe, K Matsuda, T Hama, T Konishi, M Furugen. Fabrication Process of High Nodular Corrosion-Resistant Zircaloy-2 Tubing, Zirconium in the Nuclear Industry: Tenth International Symposium. 1245 (1994) 285-306.

[11] H Abe, M Furugen. Method of evaluating workability in cold pilgering of zirconium alloy tube, Mater.Trans. 51 (2010) 1200-1205.

[12] H Abe, M Furugen. Method of evaluating workability in cold pilgering, J.Mater.Process.Technol. 212 (2012) 1687-1693.

[13] M Furugen, C Hayashi. Application of the theory of plasticity of the cold pilgering of tubes, Journal of Mechanical Working Technology. 10 (1984) 273-286.

[14] M Harada, A Honda, S Toyoshima. Simulation of cold pilgering process by a generalized plane strain FEM, J.ASTM Int. 2 (2005) 251-264.

[15] E Girard, R Guillén, P Weisbecker, M François. Effect of plastic shearing on damage and texture on Zircaloy-4 cladding tubes: Experimental and numerical study, J.Nucl.Mater. 294 (2001) 330-338.

[16] P Montmitonnet, D Farrugia, JL Aubin, F Delamare. Internal surface roughness of cold pilgered zircaloy tubes, Wear. 152 (1992) 327-342.

[17] H Abe. A New Fabrication Process for Zr-Lined Zircaloy-2 Tubing, ASTM Spec.Tech.Publ. (2000) 425-459.

[18] H Li, D Wei, H Zhang, H Yang, D Zhang, G Li. Tooling design–related spatial deformation behaviors and crystallographic texture evolution of high-strength Ti-3Al-2.5 V tube in cold pilgering, The International Journal of Advanced Manufacturing Technology. 104 (2019) 2851-2862.

[19] J Kearns. Thermal expansion and preferred orientation in zircaloy (LWBR Development Program). (1965).

[20] CS Cook, GP Sabol, KR Sekera, SN Randall, Texture control in Zircaloy tubing through processing, ASTM Spec Tech Publ. (1991) 80-95.

[21] H Abe, T Nomura, Y Kubota. Lubrication of tube in cold pilgering, J.Mater.Process.Technol. 214 (2014) 1627-1637.

[22] A Azushima, J Kibara, I Gokyu. An analysis and measurement of oil film thickness in cold sheet rolling - an investigation into friction and lubrication in cold rolling III. J.JAPAN SOC.TECHNOL.PLAST. l9 (1978) 958-965.

[23] H Yoshida, T Matsui, T Otani, K Mandai, H Kudo. EXPERIMENTAL INVESTIGATION OF THE COLD PILGERING OF COPPER TUBES. Ann CIRP. 24 (1975) 191-196.

[24] H Abe, T Iwamoto, Y Yamamoto, S Nishida, R Komatsu. Dimensional accuracy of tubes in cold pilgering, J.Mater.Process.Technol. 231 (2016) 277-287.

[25] D Crampton. Internal stress and season cracking in brass tubes, TRANS METALL SOC AIME. 89 (1930) 233-255.

[26] Z- Ding, P Huml, W Yang. Evaluation of strain hardening parameters, J.Iron Steel Res.Int. 11 (2004) 38-46.

[27] Z Ding, P Huml. Influence of stress path change on the resistance to plastic deformation of cold rolled sheets, J Univ Sci Technol Beijing Eng Ed. 12 (2005) 521-526.

[28] P Huml, PO Strandell. Utilization of Flow Stress in Metal Forming Calculations, CIRP Ann.Manuf.Technol. 33 (1984) 147-149.

[29] P Montmitonnet, R Logé, M Hamery, Y Chastel, J- Doudoux, J- Aubin. 3D elastic-plastic finite element simulation of cold pilgering of zircaloy tubes, J.Mater.Process.Technol. 125-126 (2002) 814-820.

[30] JL Aubin, E Girard, P Montmitonnet. Modeling of damage in cold pilgering, Zirconium in the Nuclear Industry: Tenth International Symposium, ASTM STP. 1245 (1994) 245-263.

[31] S Mulot, A Hacquin, P Montmitonnet, J- Aubin. A fully 3D finite element simulation of cold pilgering, J.Mater.Process.Technol. 60 (1996) 505-512.

[32] E Vanegas-Márquez, K Mocellin, L Toualbi, Y de Carlan, RE Logé. A simple approach for the modeling of an ODS steel mechanical behavior in pilgering conditions, J.Nucl.Mater. 420 (2012) 479-490.

[33] J Martin, Methods, Models, and Assumptions Used in Finite Element Simulation of a Pilger Metal Forming Process, ASME Pressure Vessels Piping Div Publ PVP. 458 (2003) 109-119.

[34] EM Mielnik. Metalworking science and engineering, McGraw-Hill, Inc.(USA), 1991,. (1991) 976.

[35] H Nakanishi, S Toyoshima, M Harada, A Honda, 3D simulations for cold pilgering process by explicit fem, Comput. Plast. - Fundam. Appl. (2009).

[36] J Hardell, B Prakash, Tribological performance evaluation of cold pilgering lubricants, (2010) 81-94.

[37] WE Carscallen, J Jeswiet, PH Oosthuizen. Optimization of a Cooling System: the Cooling of Pilgered Seamless Tubes, CIRP Ann.Manuf.Technol. 43 (1994) 223-227.

[38] J Hardell. Tribology in Cold Pilgering, (2005).

[39] D Kuznetsov. Influence of friction on the surface quality of cold-deformed pipe, Steel in Translation. 42 (2012) 447-451.

[40] C McConnell, J Lenard. Friction in cold rolling of a low carbon steel with lubricants, J.Mater.Process.Technol. 99 (2000) 86-93.

[41] B Verlinden, J Driver, I Samajdar, RD Doherty, Thermo-mechanical processing of metallic materials, Elsevier 2007.

[42] H Kim, N Kardes. Friction and lubrication, Sheet Metal Forming-Fundamentals: ASM International. (2012).

[43] https://www.bruker.com/en/products-and-solutions/test-and-measurement/tribometers-and-mechanical-testers/stribeck-curves-in-reciprocating-test.html,.

[44] UJ Möller, U Boor, Lubricants in operation, Wiley 1996.

[45] V Meinders, J Hol, A van den Boogaard, JW Yoon, TB Stoughton, B Rolfe, et al., Boundary and mixed lubrication friction modeling under forming process conditions, 1567 (2013) 912-917.

[46] E Siebel, FW Neumann. Das kaltpilgern von rohren -versuchergebniße und untersuchungen über dem walzvorgang, Stahl und Eisen. 74 (1954) 139-145.

[47] A Geleji. Die Berechnung der Kräfte und des Leistungsbedarfs beim Kaltpilgern von Rohren, Acta Techn.Ac.Sci.Hung.Budapest. 11 (1955) 461-478.

[48] J Osika, W Libura. Mathematical model of tube cold rolling in pilger mill, J.Mater.Process.Technol. 34 (1992) 325-332.

[49] R Fogelholm, P Huml, A Salwén, PILGER - Simulation Program for Cold Pilger Rolling, Unpublished confidential report. (1991).

[50] J Osika, H Palkowski, K Swiatkowski, D Pociecha, A Kula. Analysis of material deformation during the new cold tube rolling process realized on the new generation of pilger mills, Arch.Metall.Mater. 54 (2009) 1239-1251.

[51] J Hitchcock. Roll neck bearings, Report of ASME Special Research Committee on Heavy-duty Anti-friction Bearings. (1935) 33-41.

[52] E Siebel, U Stahl. Eisen. 45 (1925) 1563.

[53] T Von Karman. On the theory of rolling, Z.Angew.Math.Mech. 5 (1925) 139-141.

[54] G Sachs. Zur Theorie des Ziehvorganges, Z.Angew.Math.Mech. 7 (1927) 235-236.

[55] JL Aubin, P Montmitonnet, S Mulot, Zirconium alloy cold pilgering process control by modeling, ASTM Spec Tech Publ. (2000) 460-481.

[56] RW Davies, MA Khaleel, WC Kinsel, HM Zbib. Anisotropic yield locus evolution during cold pilgering of titanium Alloy Tubing, J Eng Mater Technol Trans ASME. 124 (2002) 125-134.

[57] B Lodej, K Niang, P Montmitonnet, J- Aubin. Accelerated 3D FEM computation of the mechanical history of the metal deformation in cold pilgering of tubes, J.Mater.Process.Technol. 177 (2006) 188-191.

[58] D Pociecha, B Boryczko, J Osika, M Mroczkowski. Analysis of tube deformation process in a new pilger cold rolling process, Arch.Civ.Mech.Eng. 14 (2014) 376-382.

[59] J Edberg. Computational modeling of hot rolling. (1996).

[60] MSC.Software, MSC.Marc Manual, Version 2013, Palo Alto, USA. (2013).

[61] T Wanheim, N Bay. A model for friction in metal forming processes, CIRP Annals-Manufacturing Technology. (1978).

[62] FP Bowden, D Tabor, The friction and lubrication of solids, Oxford university press 2001.

[63] Z Jiang, A Tieu, X Zhang. Finite element modelling of mixed film lubrication in cold strip rolling, J.Mater.Process.Technol. 151 (2004) 242-247.

[64] PE Armstrong, JE Hockett, OD Sherby. Large strain multidirectional deformation of 1100 aluminum at 300 K, J.Mech.Phys.Solids. 30 (1982) 37-58.

[65] Frost, H. J., Ashby,M.F., Deformation-mechanism maps : the plasticity and creep of metals and ceramics, Pergamon Press, Oxford [Oxfordshire]; New York, 1982.

[66] RA Lebensohn, MI González, CN Tomé, AA Pochettino. 1.4. Mechanical behavior: Measurement and prediction of texture development during a rolling sequence of Zircaloy-4 tubes, J.Nucl.Mater. 229 (1996) 57-64.

[67] NP Gurao, H Akhiani, JA Szpunar. Pilgering of Zircaloy-4: Experiments and simulations, J.Nucl.Mater. 453 (2014) 158-168.

[68] J Singh, S Mahesh, G Kumar, P Pant, D Srivastava, GK Dey, et al. Texture Development and Plastic Deformation in a Pilgered Zircaloy-4 Tube, Metall Mat Trans A Phys Metall Mat Sci. 46 (2015) 1927-1947.

[69] H Li, D Wei, H Zhang, H Yang, H Liu, S Liu, et al. Texture evolution and controlling of high-strength titanium alloy tube in cold pilgering for properties tailoring, J.Mater.Process.Technol. 279 (2020) 116520.

[70] DC Stouffer, LT Dame, Inelastic deformation of metals : models, mechanical properties, and metallurgy, Wiley, New York, 1996.

[71] R Hill. A theory of the yielding and plastic flow of anisotropic metals, Proc.Roy.Soc.London. 193 (1948) 281-297.

[72] E Vanegas-Márquez. “Numerical Modeling of ODS Steels Tubes Pilgering,” PhD Thesis, Ecole Nationale Supérieure des Mines de Paris. (2011).

[73] D Sornin, EA Pachón-Rodríguez, E Vanegas-Márquez, K Mocellin, R Logé. Numerical Modeling of Tube Forming by HPTR Cold Pilgering Process, J Mater Eng Perform. 25 (2016) 4059-4069.

[74] S Deng, H Song, C Zheng, S Zhang, L Chu. A model to describe hardening behavior of Zircaloy-4 tube during cold pilgering process, International Journal of Material Forming. (2018) 1-9.

[75] Z Chu, D Wei, L Jiang, D Zhang, Q Huang, Y Li. Numerical model establishment and verification of cold pilgering on cycle feed rate, J.Iron Steel Res.Int. 25 (2018) 398-408.

[76] PJ Armstrong, C Frederick, A mathematical representation of the multiaxial Bauschinger effect, Central Electricity Generating Board [and] Berkeley Nuclear Laboratories … 1966.

[77] P Huml, R Fogelholm, A Salwén. Optimization of Cold Rolling of Precision Tubes, CIRP Ann.Manuf.Technol. 42 (1993) 283-286.

[78] P Huml, R Fogelholm. Simulation model of cold pilgering, J.Mater.Process.Technol. 42 (1994) 167-173.

[79] Y. Azizoğlu and L-E. Lindgren. Temperature and plastic strain dependent Chaboche model for 316L used in simulation of Cold Pilgering (Submitted for publication), .

Department of Engineering Sciences and Mathematics
Division of Solid Mechanics

ISSN 1402-1544
ISBN 978-91-8048-293-6 (print)
ISBN 978-91-8048-294-3 (pdf)

Luleå University of Technology 2023

LULEÅ
UNIVERSITY
OF TECHNOLOGY